Sustainable and Resilient Infrastructure

ISSN: 2378-9689 (Print) 2378-9697 (Online) Journal homepage: www.tandfonline.com/journals/tsri20

Seismic vulnerability assessment of skewed concrete I-girder bridges considering various structural systems

H. Kiarad, M. M. Memarpour, S. Soltanieh & P. E. Mergos

To cite this article: H. Kiarad, M. M. Memarpour, S. Soltanieh & P. E. Mergos (01 Aug 2025): Seismic vulnerability assessment of skewed concrete I-girder bridges considering various structural systems, Sustainable and Resilient Infrastructure, DOI: 10.1080/23789689.2025.2540129

To link to this article: https://doi.org/10.1080/23789689.2025.2540129

Published online: 01 Aug 2025.

SUSTAINABLE AND RESILIENT INFRASTRUCTURE
https://doi.org/10.1080/23789689.2025.2540129

Taylor & Francis
Taylor & Francis Group

Seismic vulnerability assessment of skewed concrete I-girder bridges considering various structural systems

H. Kiarad[a], M. M. Memarpour[b], S. Soltanieh[c] and P. E. Mergos[c]

[a]Department of Civil Engineering, Imam Khomeini International University, Qazvin, Iran; [b]Department of Civil Engineering, Faculty of Engineering and Technology, Imam Khomeini International University, Qazvin, Iran; [c]Department of Civil Engineering, CITY ST GEORGE'S, University of London, London, UK

ABSTRACT

The present study examines, for the first time, the combined effects of structural systems and skew angles on the seismic response of multi-span reinforced concrete I-girder bridges. For this purpose, two prevalent superstructure systems, namely, multi-span simply supported and multi-span continuous, are considered. For each system, the boundary conditions at the superstructure–substructure interface are modeled assuming elastomeric bearings with steel dowels. In the case of the multi-span continuous systems, two more commonly applied types of bent-to-deck connections are considered, including pinned connectivity and elastomeric bearings without steel dowels. To account for the irregularity, five skew angles ranging from 0° to 60° are also considered. Probabilistic seismic demand models are developed for key components, such as columns and bearings, and subsequently, component- and system-level fragility curves are generated. The results reveal that skew angle variation can influence the bridge system fragility by up to 40% across different structural systems.

ARTICLE HISTORY
Received 24 September 2024
Accepted 23 July 2025

KEYWORDS
Concrete I-girder bridge; skewness; structural irregularity; fragility curves; seismic vulnerability assessment

1. Introduction

Recently, there has been a controversial issue regarding the extent to which employing different types of structural systems affects the seismic response of highway bridges (Sun et al., 2023). In bridges, the load transition path between the superstructure and substructure is affected by the type of pier-to-bent connection (Ishac & Mehanny, 2016). Consequently, it is imperative to assess the influence of various structural systems and connections on the seismic response of bridges. Several studies can be found in the literature that investigate the impact of different structural systems on a bridge under seismic excitations (Abbasi & Moustafa, 2017; Abbiati et al., 2018; Abdelnaby et al., 2014). For example, Hou et al. (2017) investigated the seismic demand of simple-made-continuous I-girder bridges with integral abutments using three types of bent-to-deck connectivity: roller, pinned, and fixed. With the intention of minimizing the moment demand at the pier base of the bridge, the pinned and roller bent-to-deck connections were found to be preferable to the fixed connections in the skewed-only configurations in low-intensity seismic zones. A recent study by Sun et al. (2023) examined two types of connection between the pier and bent on a small-radius curved bridge: one with a monolithic pier-to-bent connection and the other with a fixed support installed at the pier-to-bent connection. They observed that the bridge model employing the latter structural system displays greater susceptibility to concrete splitting failure during seismic excitations in comparison to that of the former one. However, previous studies did not specifically address the effects of various structural systems, including multi-span simply supported and multi-span continuous, on the seismic vulnerability assessment of seismically designed concrete I-girder bridges with seat-type abutments. Furthermore, in the latter system, they did not investigate the effects of bent-to-deck connections, including pinned connectivity and elastomeric bearings without steel dowels.

On the other hand, skewed bridges are widely acknowledged as the best solution to deal with the geometric restrictions associated with some regions in which regular (straight) configurations cannot be

CONTACT P. E. Mergos panagiotis.mergos.1@city.ac.uk

accommodated due to complex terrain (Miner, 2014). Such situations necessitate adopting bridges with skew-angled bents and/or seat-type abutments in order to overcome the geometrical constraints or in other sense costly construction and easing traffic flow. In addition, the shift from a regular bridge to an irregular one, characterized by skew angles exceeding 20° (Caltrans, 2019), inherently adds to the complexities of the seismic assessment problems. For example, large earthquakes such as Chile (2010) resulted in deck unseating or displacement of superstructure, particularly evident in skewed bridges (Elnashai et al., 2012).

Over the last 25 years, many researchers have extensively studied the seismic behavior of skew bridges (Abbasi & Moustafa, 2019; Aldea et al., 2021; Kaviani, Zareian, & Taciroglu, 2012; Omranian, Abdelnaby, & Abdollahzadeh, 2018; Sullivan & Nielson, 2010; Yang, Werner, & DesRoches, 2015; Zakeri, Padgett, & Amiri, 2014; Zakeri & Zareian, 2018). Their focus has been on the seismic assessment of skewed bridges, aiming to uncover vulnerabilities related to the structural components of bridges. Generally, it is observed that increasing the skew angle of the bridge superstructure alters the seismic behavior of reinforced concrete (RC) bridges as a result of coupling translational modes with rotational modes of vibration. Through cloud analysis, Noori et al. (2019) evaluated the seismic vulnerability of a skewed two-span RC I-girder bridge with a pinned bent-to-deck connection. It was indicated that as the skew angles vary from 0° to 60°, the seismic fragility of the column has been mitigated. In a study conducted by Huo and Zhang (2013), the seismic performance of RC highway bridges was perused under the combined effects of pounding and skewness. Their findings showed that when pounding did not occur, the seismic performance of the columns in skewed bridges outperformed that of straight bridges as the skew angle increased. Notwithstanding the extensive research on skewed bridges, none of the aforementioned works specifically inspected how various structural systems affect the seismic vulnerability assessment of skewed I-girder bridges.

The novelty of this research is to evaluate the simultaneous effects of structural systems and skew angles on the seismic response of RC I-girder bridges. In the present research, four unique combinations of superstructure systems and bent-to-deck connections are generated. To this end, two types of commonly used bridge superstructure systems, including multi-span simply supported I-girder and multi-span continuous I-girder, are studied. Additionally, two commonly applied connections in the case of continuous I-girder superstructures, namely, pinned connectivity and plain elastomeric bearings (also referred to as unreinforced elastomeric bearings or elastomeric bearings without steel dowels), are considered. In addition, the angle of skewness varies between 0° and 60° with increments of 15°. Therefore, 20 different structural configurations of I-girder bridges are generated. For nonlinear time history analysis (NLTHA), finite element models of the bridges are created, and a set of bidirectional horizontal far-field ground motions is selected. A total of 800 NLTHAs are conducted on the bridge models using the OpenSEES platform. To compare seismic vulnerability of the most important components, such as columns and bearings, fragility assessment is implemented at four different limit states by developing probabilistic seismic demand models for each bridge model. Subsequently, the system-level fragility of all bridge models is derived through joint probabilistic demand models. Lastly, this paper ends with notable findings and recommendations for future research.

2. Structural systems

In this research, different types of structural systems applied to concrete I-girder bridges are studied based on their capabilities in transferring loads between the super- and substructure. Two commonly used types of bridge superstructure systems are studied: multi-span simply supported I-girders (MSSS) and multi-span continuous I-girders (MSC). The MSSS and MSC structural systems are distinguished by the presence of a gap between adjacent decks at the bents for the former case. The MSSS structural system entails discrete spans with joints, allowing each span to act independently in response to seismic loads. In contrast, in the MSC superstructure, the bridge spans are connected without any expansion joints. For each system, the boundary conditions at the superstructure–substructure interface are modeled assuming elastomeric bearings with steel dowels. Additionally, two prevalent connectivity types in MSC superstructures are examined: pinned connectivity and plain elastomeric bearings. Overall, the structural systems are categorized as multi-span simply supported (MSSS) (Bhaskar Panchireddi & Ghosh, 2023; Ghosh, 2021), multi-span continuous with fixed and expansion bearings (MSC-FEB) (Ghosh, 2021; Yang, Werner, & DesRoches, 2015), multi-

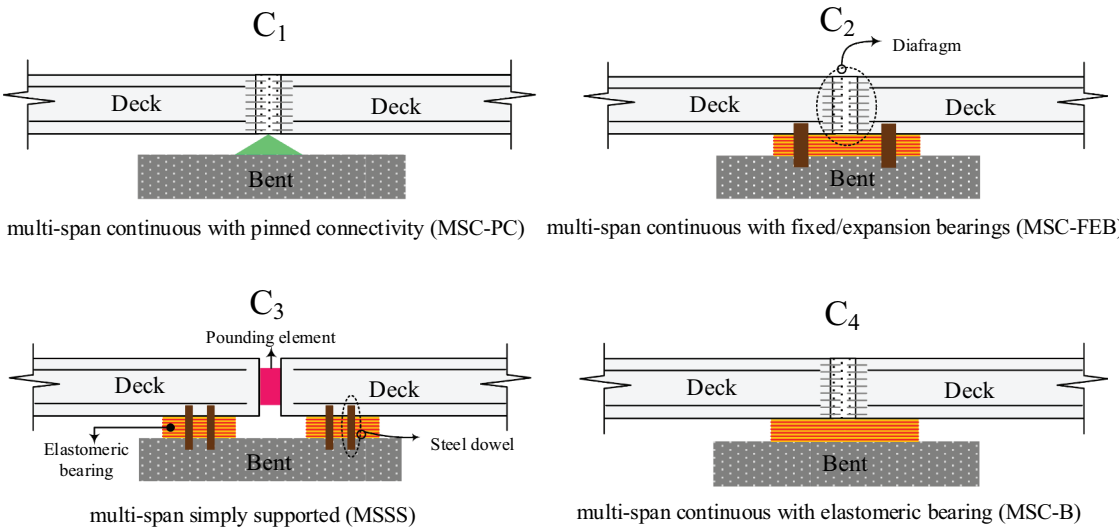

Figure 1. General view of the various structural systems for multi-span I-girder bridge, with associated designations.

span continuous with elastomeric bearings (MSC-B) (Mirzai et al., 2023; Zakeri & Ghodrati Amiri, 2014), and multi-span continuous with pinned connectivity (MSC-PC) (Soltanieh, Memarpour, & Kilanehei, 2019). Figure 1 provides a general view of the various structural systems for multi-span RC I-girder bridges. To simplify the notation, each case of the structural systems is denoted by the letter 'C' with a numerical subscript. Accordingly, MSC-PC (no fixed/expansion bearings at bents), MSC-FEB, MSSS, and MSC-B are indicated as C_1, C_2, C_3, and C_4 hereafter. The four structural systems and their corresponding designations are summarized in Figure 1.

The way in which loads are transferred between the superstructure and substructure of bridges is heavily influenced by the type of structural system. The C_1 structural system allows free relative rotation between the superstructure and the substructure about all axes at the bent. In other words, this structural system transfers all translational forces from the superstructure (deck girders) to the substructure (cap beam) without moment transfer. In the case of C_4, there is no moment transfer between the superstructure and the substructure at the bent either, and the seismic translational loads transfer via bearings. Although the seismic load path for both the C_2 and C_3 systems is similar to that of the C_4 structural system, the movement of the superstructure of the two former systems is restricted by steel dowels. This occurs once the steel dowels engage with the elastomeric bearing.

3. Models of bridges

3.1. Bridge geometric characteristics

Multi-span I-girder reinforced concrete (RC) bridges are a widely constructed structural design found across the globe (Jankowski, 2015; Kabir, Billah, & Alam, 2019; Shekhar, Ghosh, & Ghosh, 2022). A schematic view of the longitudinal elevation and transverse cross-section of the bridge, as well as the arrangement of bearing types across various structural systems is represented in Figure 2. The bearing types are identified by distinct symbols: fixed bearing (orange triangle), expansion bearing (green circle), bearing without steel dowels (pink circle), and pinned connection (blue triangle). The bearing characteristics are discussed in §3.2. The superstructure has a length of 48.8 m and a width of 15.01 m. The superstructure is composed of a middle span with length of 24.4 m, and two side spans with length of 12.2 m. The bridge deck is constituted of eight concrete girders and a concrete slab on top with a thickness of 0.178 m. AASHTO girder types of I and III girders are used for the side spans and middle-span. The side spans are supported by seat-type abutments at one end and a three-column bent at the other. The abutments rest on batter and vertical-type pile foundations, while the bent is attached to three eight-pile foundations. Backwall with a height of 2.4 m is accounted for embankment. Clayey backfills are also assumed for the abutment

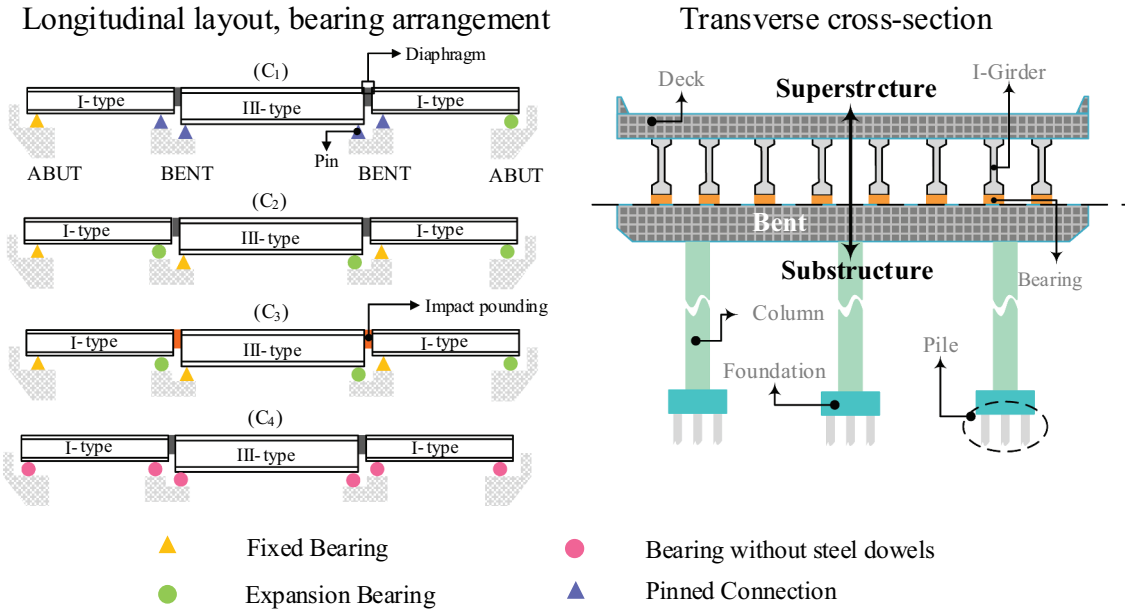

Figure 2. Schematic view of a typical multi-span RC I-girder bridge with bearing distribution across structural systems.

backwall. Typically, the gap between abutment and deck is 25.4 mm, while the gap between adjacent decks is 38.1 mm.

Columns of the bridge have a circular section with a diameter of 0.914 m and a height of 4.6 m. They are connected at the top using a cap beam of rectangular section with a width of 1.07 m and depth of 1.22 m, as the columns are also tied at the bottom using a pile cap. The center-to-center distance of columns at bent is 5 m. This circular column comprises 12 #29 longitudinal rebars. Moreover, #13 stirrups with a spacing of 76 mm on center (#13 bars @ 76 mm o.c.) are transversely distributed along the column, resulting in a ductile column (K. Ramanathan, Desroches, & Padgett, 2012). This implies seismically designed columns, whereby the flexural mode predominates in the column. Cross-section and elevation view of the seismically designed reinforced concrete bridge column are illustrated in Figure 3.

It should be noted that only neoprene pads (elastomeric bearings) are used in the C_4 structural system without any steel dowels beneath the concrete girders, whereas the concrete girders of the three other structural systems are integrated into elastomeric bearings utilizing steel dowels, i.e., fixed and expansion bearings. The fixed and expansion bearings are constructed by embedding two steel dowels with a diameter of 25.4 mm above the concrete cap beam and/or abutment. It is done by passing the steel dowels through the circular holes within the elastomeric bearings for the fixed bearings and slotted holes for the expansion bearings. The dimensions of the slotted hole are 31.8 mm × 76.2 mm, and the diameter of the circular hole is 31.8 mm. Moreover, the steel dowel must be inserted into a 76.2 mm hole in the bottom of the girder such that the steel dowel can move loosely inside the hole. In the case of I-type girders, the elastomeric bearing pads are 406 mm wide and 152 mm long with a thickness of 25.5 mm. In the case of III-type girders, the dimensions are 559 mm × 203 mm × 25.5 mm. The only difference between the fixed and expansion bearings is the gap between the elastomeric bearing pad and the steel dowel, which is 3.2 mm and 25.4 mm, respectively, along the longitudinal axis. In contrast, an identical gap size of 3.2 mm is considered for both types of bearings along the transverse direction.

The geometric configuration of the bearings and the steel dowel holes are illustrated in Figure 4. Because the deck is prone to unseating during seismic events, the steel dowels serve as restraining devices to prevent excessive movement of the girders that are seated on elastomeric bearings. Besides, to protect the bridge from potential movements such as anticipated thermal expansion, gap-defined holes are implemented to relieve stresses in the bent/abutment (Maleki, 2005). In total, 96 steel dowels resided in 48 elastomeric bearing pads throughout the bridge where the superstructure meets the supports for C_3 and C_2. Similarly, in the same order, 32 steel dowels and 16 elastomeric bearing pads are needed for C_1, whereas only 48 elastomeric bearing pads are required

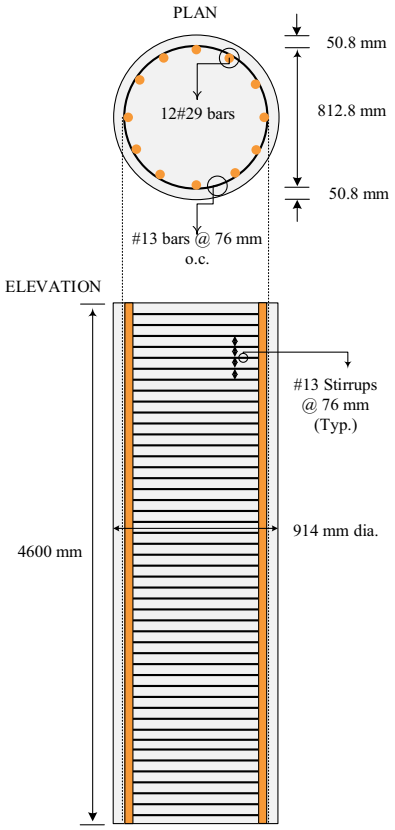

Figure 3. Cross-section and elevation view of the seismically designed reinforced concrete bridge column.

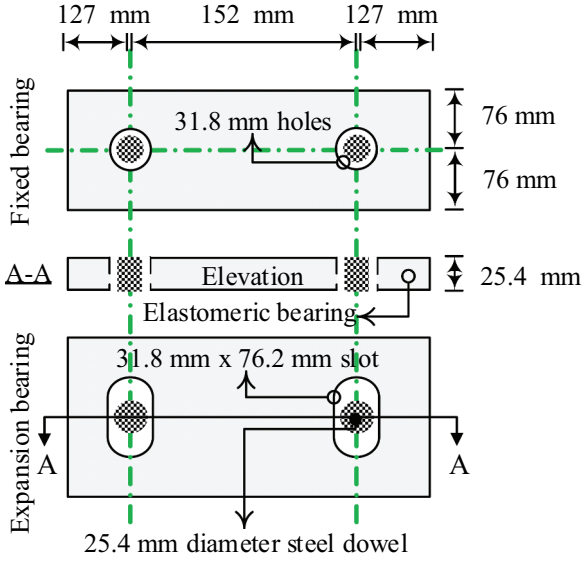

Figure 4. Plan and elevation view of the fixed and expansion bearings with steel dowels.

for C_4. When the steel dowel acts elastically, the combination of the steel dowel and elastomeric bearing restricts the motion of girders. If the steel dowel breaks under strong dynamic excitation, the only governing factor between the girder and bearing is sliding due to the elastomeric bearing. Furthermore, such bearings are immune against walking out, contingent on being properly secured in place. Detailed information about the geometric properties of the bridge can be found in (Nielson, 2005).

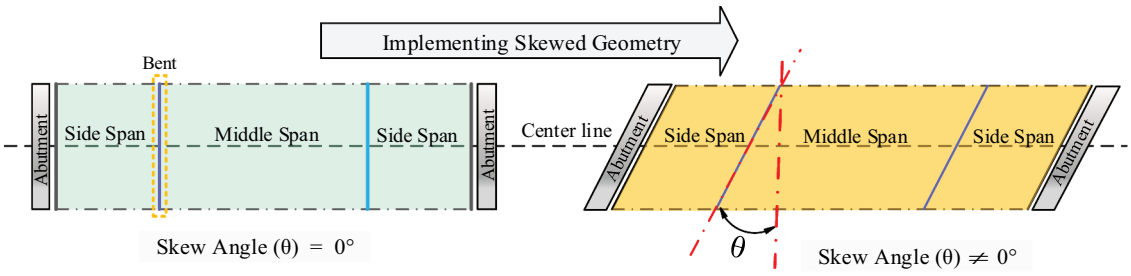

Figure 5. Geometric configuration of the straight/skewed concrete I-girder bridge system.

For implementing skewed geometry in the bridge, angular increments of 15° (ranging from 0° to 60°) are adopted (Mangalathu, Jeon, & Jiang, 2019; Noori et al., 2019; Rezaei, Mohammadi Dehcheshmeh, & Tsompanakis, 2025; Somala, Karthik Reddy, & Mangalathu, 2021). Figure 5 compares the bridge configurations with straight ($\theta = 0°$) and skewed ($\theta \neq 0°$) geometries.

3.2. Finite element modeling

Nonlinear three-dimensional finite element models of the bridge are developed in OpenSEES (McKenna, 2011). It is assumed that the superstructure remains elastic during seismic excitations. Therefore, the deck is modeled using elastic beam-column elements at the center along the longitudinal direction. Geometric and mechanical properties of the deck are calculated and assigned to these elastic elements. Nodal mass is defined on superstructure nodes. The nonlinear behavior of columns is modeled by displacement-based beam-column elements and discretized fiber sections. The stress-strain laws of materials used to model confined and unconfined concrete are based on the work of Terzic and Stojadinovic (2015), and the maximum compressive strength is calculated by means of equations proposed by Mander, Priestley, and Park (1988). In OpenSEES, both the confined and unconfined behaviors are modeled using Concrete01 in which the ultimate concrete compressive strains are 0.062 and 0.0055. Besides, reinforcing steel is modeled using Steel01. At the top of the columns, the bent is modeled using a nonlinear beam-column element and a quadrilateral fiber section. The foundation system at the bottom of the columns is also simulated by means of linear translational and rotational springs. In abutments, it is important to note that the piles and the surrounding soil both participate in passive resistance, whereas the piles alone contribute to the active resistance. Additionally, the transverse direction resistance is only provided by piles without taking into account the resistance of wing walls. According to Shamsabadi and Rollins (2014), the HyperbolicGap material is used to model the nonlinear behavior of the abutment back-wall soil. To simulate piles, a trilinear model recommended by Choi (2002) is adopted. Furthermore, an impact element is defined through a bilinear model for deck-to-deck/deck-to-abutment collisions according to the recommendation of Muthukumar and DesRoches (2006). The energy dissipation of pounding is also considered in the model. A schematic view is presented in Figure 6 illustrating the arrangement and behavior of all the components utilized in the analytical model of the bridge in OpenSEES.

The fixed and expansion bearings are composed of an elastomeric bearing and two steel dowels. Seven steps are involved in the modeling of these bearings. Step 1: the elastomeric bearings associated with I-girder and III-girder are modeled using an elastic perfectly plastic material that has an initial stiffness of 3.4 kN/mm and 6.2 kN/mm, respectively. Step 2: the behavior of the steel dowel is modeled using a hysteretic material with an initial stiffness of 92 kN/mm. Step 3: to account for the gap in the bearings, an elastic perfectly plastic gap material with an initial stiffness of 92 kN/mm is defined. Then, the hysteretic material modeled in step 2 is connected in series to the elastic perfectly plastic gap material with a positive initial gap, e.g., +3.2 mm for the longitudinal fixed bearing, resulting in the tension behavior of the steel dowel considering the positive gap. Step 4: step 3 is repeated with a negative initial gap, in order to achieve the compression behavior of the steel dowel considering the negative gap (−3.2 mm). Step 5: through the parallel connection of the systems of springs created in steps 3 and 4, the cyclic behavior of steel dowels considering two-sided gaps is modeled. Step 6: the hysteretic behavior of the longitudinal fixed bearing is made by combining in parallel the resulting

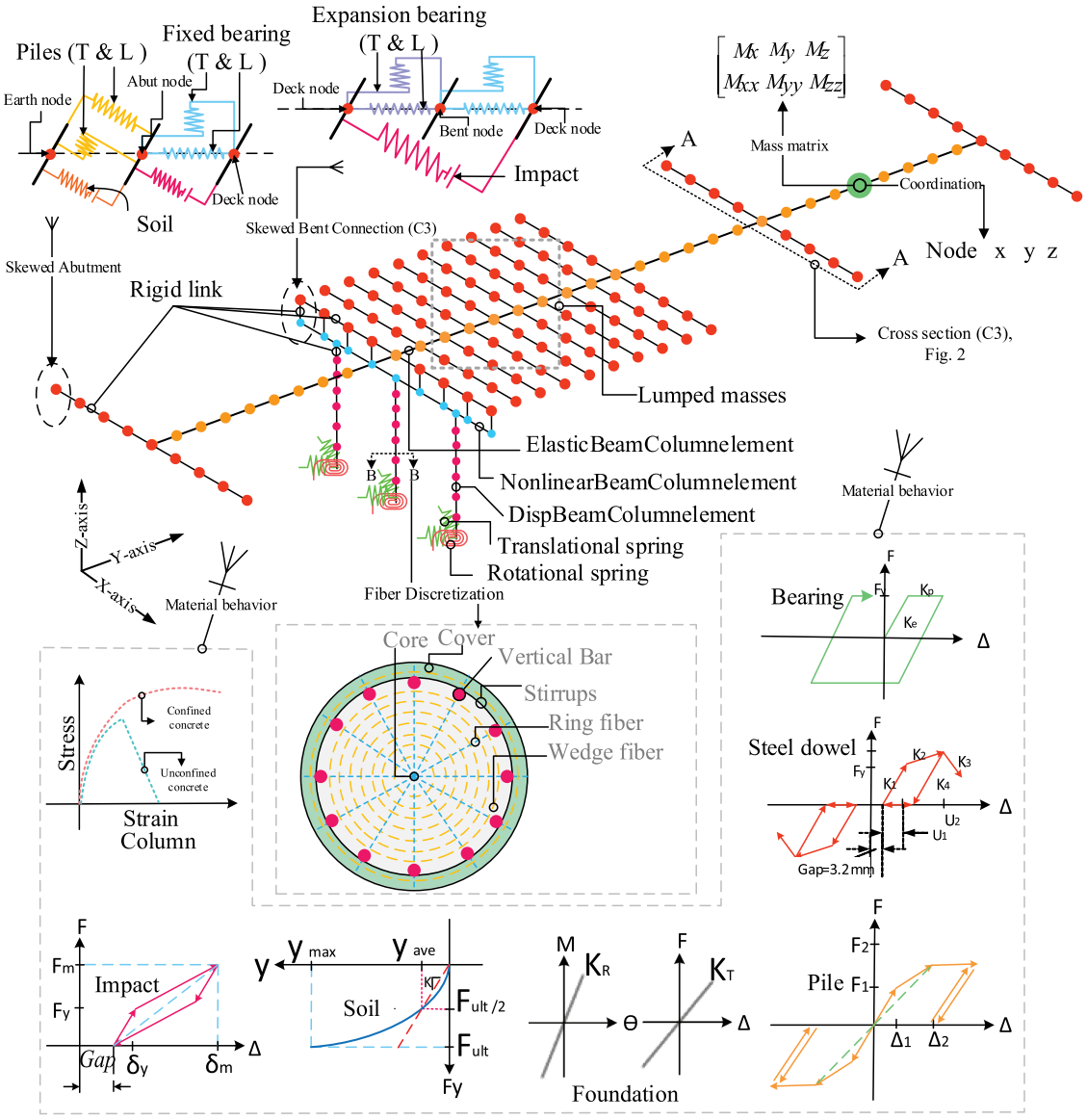

Figure 6. Analytical model of bridge.

system of springs from step 1 with that of step 5. Step 7: the resultant material generated in step 6 is applied to a zero-length element connecting the nodes between the deck and bent/abutment. The expansion bearing is also modeled in a similar way to the fixed bearing.

As mentioned in §3.1, the only difference between fixed and expansion bearings is the size of the gap at which the steel dowels can freely move until the closure of the gap. Once the gap in the fixed and expansion bearings is closed, engagement between the steel dowel and elastomeric bearing is incurred. Consequently, this engagement is postponed by the time delay associated with the size of the gap. In this research, interaction between steel dowels and elastomeric bearings is overlooked.

In C_1, the translational degrees of freedom (DOFs) of the super- and substructure nodes are equalized while the rotational DOFs are free to rotate. In the modeling of the others, such as C_2, only the vertical translational direction DOF of the superstructure node is equalized to that of the cap beam, and the rotational DOFs can rotate freely. In case of C_2 and C_3, the deck is connected to the cap beam using a zero-length element and the materials defined earlier in this section (i.e., fixed and expansion bearings). Furthermore, C_4 is quite similar to C_2 with the only difference that steel dowels are eliminated in the model of C_4. It should be noted that in seat-type abutments, the gap and the pounding between the superstructure deck and the abutment need to be addressed correctly. In this manner, the longitudinal

bearings are deployed parallel to the impact element in the abutment as well as in series with the soil element. The placement of bearing types along the bridge length can be seen in Figure 2.

A pushover analysis is conducted on the three-dimensional finite element model of the straight bridge assuming C_1. Figure 7 illustrates the monotonic moment-curvature behavior of the circular fiber-defined section of the column along the longitudinal direction. A cyclic analysis is also conducted in order to demonstrate the cyclic behavior of the column and bearings. The relationship between the moment and curvature of the column can be seen in Figure 8(a). The hysteretic behavior of the force-deformation related to the longitudinal fixed and expansion bearings is also illustrated in Figure 8(b,c), respectively.

As opposed to straight bridges, skewed bridges are built with skewed-angle bents and/or seat-type abutments. In this regard, finite element models of skewed bridges contain additional rigid elements along the transverse axis to account for skewness effects on seismic responses of bridges. The transverse deck elements are rotated in accordance with the desired skew angle of the bridge, which produces an angle of θ other than 90° with respect to the longitudinal deck elements (i.e., parallel to the traffic direction). Additionally, the implementation of skew angles into the finite element models necessitates alterations to the orientation of several bridge elements. These elements are related to the piles and their surrounding soil, including impact, soil, and pile springs at the abutments, and rotational and translational springs at the foundation. These elements are required to be adjusted in accordance with the implemented skew angle of the bridge. To model skewed C_3 bridges, the orientation of the impact element at adjacent decks is also modified such that it is normal to the decks. Nonetheless, all bearings, including the fixed and expansion bearings as well as the bearings without steel dowels, remain unchanged for models across all skew angles such that their orientations are collinear with the bridge principal axes.

The deck of skewed bridges under seismic excitation tends to rotate in-plane about its vertical axis and subsequently, the skewed superstructure separates from the abutment at the acute corner while binding at the obtuse corner. This phenomenon leads to the creation of an inherently asymmetric passive wedge inside

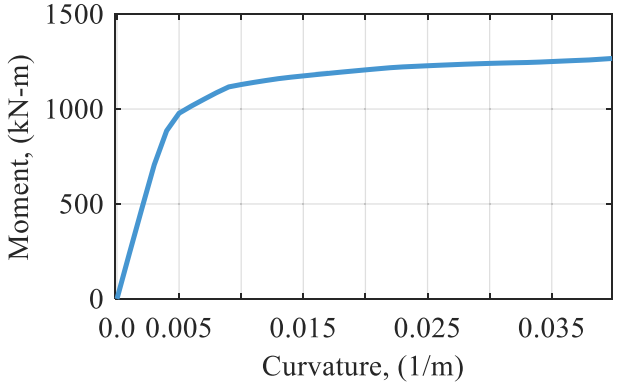

Figure 7. Pushover analysis on column along longitudinal direction (Monotonic moment-curvature behavior of column).

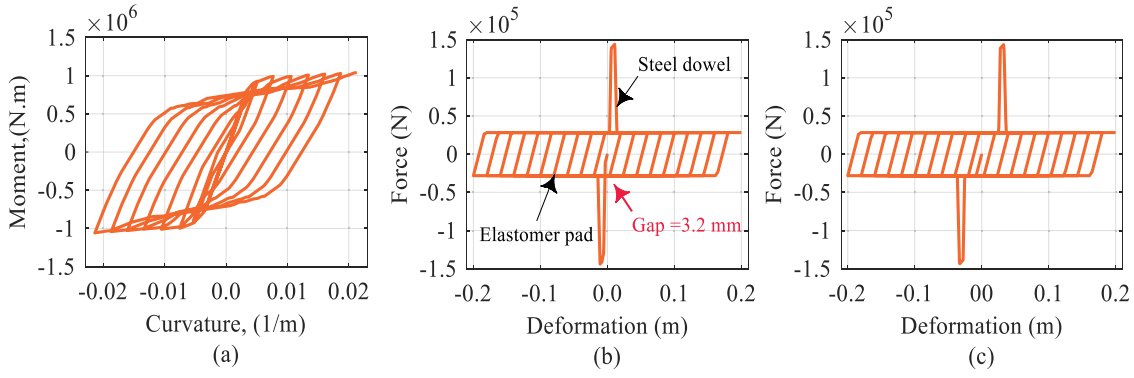

Figure 8. Cyclic analysis response along longitudinal axis for (a) Moment-curvature relationship of column, (b) Fixed bearing, and (c) Expansion bearing.

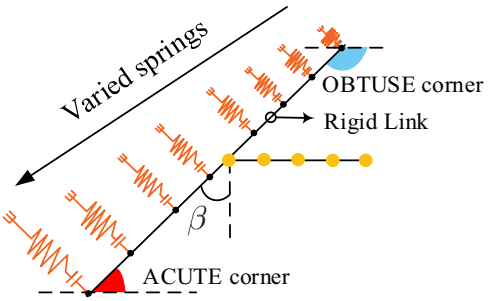

Figure 9. Soil springs simulation for skewness.

the abutment backfill (Shamsabadi & Rollins, 2014). In addition, the volume of backfill soil mobilized per unit length of the abutment wall increases from the obtuse corner to the acute corner. For analytical models of skewed abutments to reflect these effects, different properties must be assigned to the nonlinear hyperbolic springs depending on their distance from the obtuse corner. The illustration of the analytical model related to skewed-angle abutments can be found in Figure 9. To consider the different properties in the soil springs, the variation coefficients of soil stiffness are calculated based on $\beta = 0.3(\tan(\theta)/\tan(60°))$, which are a function of the skew angles (Kaviani, Zareian, & Taciroglu, 2012), and are postulated at both abutments during the skewing process. In skewed bridges, there is also the potential for the decks to rub against each other due to the addition of skew, but in the simulation process, this can be ignored assuming the frictional resistance is substantially lower than the impact stiffness of the surfaces (Saiidi et al., 2013). In this study, five different skew angles of 0°, 15°, 30°, 45°, and 60° are selected to investigate the skewness impacts on seismic responses of RC I-girder bridges. Each case of skew angles is represented by the letter 'S' with a numerical subscript for simplicity. Hereafter, S_1 to S_5 are representatives of 0° to 60° angles of skew with increments of 15°. It should be noted that structural responses are influenced by modeling assumptions (De Matteis et al., 2022; Engen et al., 2017). For example, the consideration of an inherently asymmetric passive wedge within the abutment backfill for skewed bridges is one of such modeling assumptions adopted in this study.

Damping proportional to the stiffness component using the updated tangent stiffness is utilized in the models in which only one mode, the first mode, is assigned to determine the damping coefficients. In the models, a 5% damping ratio is assumed. In the present study, seismic excitations are imposed on the fixed nodes of the soil springs (i.e., HyperbolicGap elements) at the abutments and the bent foundation springs (i.e., linear translational and rotational elements).

4. Dynamic bridge characteristics

The dynamic characteristics of the bridge models with the different structural systems and skew angles are determined through eigenvalue analysis. The periods of the first and the second modes of vibration are presented in Table 1 for the 20 bridge models. In the table, C_2S_3 denotes the bridge model with the MSC-FEB structural system (C_2) and a skew angle of 30° (S_3). This table shows that the elastic period of the first vibration mode is longer than that of the second vibration mode for all the models. The fundamental mode of a straight bridge is characterized by a mode shape that is predominantly in the longitudinal direction.

Table 1. Periods (s) of the first and the second modes of vibration.

		Skew angles									
		S_1		S_2		S_3		S_4		S_5	
		1st	2nd	1st	2nd	1st	2nd	1st	2nd	1st	2nd
Structural systems	C_1	0.548	0.373	0.548	0.373	0.548	0.373	0.549	0.373	0.550	0.374
	C_2	0.559	0.435	0.572	0.445	0.573	0.445	0.574	0.445	0.575	0.445
	C_3	0.635	0.484	0.646	0.488	0.659	0.484	0.670	0.480	0.670	0.477
	C_4	0.559	0.435	0.572	0.445	0.573	0.445	0.574	0.445	0.575	0.445

According to the table, the fundamental periods for the regular realizations of the bridge models are 0.548 s, 0.559 s, 0.635 s, and 0.559 s corresponding to C_1, C_2, C_3, and C_4, respectively. The bridge model with the C_1 structural system is inherently stiffer than the bridge model with discontinuous superstructure and fixed/expansion bearings, C_3, in which the fundamental period is the highest among the structural systems. In the case of C_1, C_2, and C_4 with S_1, the second mode shape oscillates in the transverse direction. However, the second mode shape of C_3S_1 exhibits side spans vibrating in both rotational and translational DOFs, while its middle span sustains significant translational motion only. Referring to the table, the periods of 0.373 s, 0.435 s, 0.484 s, and 0.435 s correspond to the second modes of C_1S_1, C_2S_1, C_3S_1, and C_4S_1.

The influence of skewness on the mode shape of the bridge can be easily understood from the periods of vibration for the first and the second modes provided in Table 1. For instance, in the C_3S_4 model, the first mode period is 0.67 s, whereas it is 0.63 s for C_3S_1. Unlike C_3S_1, the first mode shape of C_3S_4 is a combination of longitudinal and transverse movements. Nevertheless, the second mode shape of C_3S_4, albeit for middle span is translational along the 45°-transverse axis of the bridge akin to that of the C_3S_1 model. However, the side spans of the C_3S_4 model demonstrate an interaction of the translational and rotational movements. Besides, the second mode periods of vibration of the straight and skewed bridges with C_3 are approximately equal, as seen with cases of C_1, C_2, and C_4. Overall, the skewed bridges show complex interaction between the first and the second modes of vibration in comparison to the straight bridges where the first mode of vibration is normally along the longitudinal direction of the bridge, and the second mode of vibration is along the transverse direction.

5. Seismic fragility function methodology

5.1. Fragility function

Following Nielson (2005) and Mangalathu, Jeon, and Jiang (2019), this study employs fragility functions to generate fragility curves. Numerous researchers have employed analytical fragility functions to assess the seismic vulnerability of skewed RC I-girder bridges (e.g., Mangalathu, Jeon, & Jiang, 2019; Soleimani et al., 2017). This paper also evaluates, in an analytical manner, the vulnerability of bridge components across different structural systems and angles of skewness. The seismic fragility function estimates the likelihood of bridge component demand reaching or exceeding a predetermined threshold at a certain level of seismic intensity. As a general description of the fragility function (conditional probability), it can be stated as follows:

$$Fragility = P\left\{\frac{D}{C} \geq 1 | IM\right\} \tag{1}$$

Where P is the probability that the seismic demand on a bridge component (D) meets or exceeds its corresponding quantified limit state capacity (C) subject to a given level of intensity measure (IM). To make it more convenient, this probability is transformed into the space of the log-normal probability distribution (Wen et al., 2003).

Based on Eq. (1), the fragility function is evaluated through a convolution of capacity models, given a limit state, and demand models. *IM*-conditioned demand models are probability distributions of structural demand, known as probabilistic seismic demand models (PSDMs). To develop PSDMs, peak responses of structural demands or engineering demand parameters (*EDPs*) obtained through NLTHAs are plotted versus the values of ground motion *IM* (e.g., peak ground acceleration). Then, utilizing the *IM-EDP* pairs and a power-law function proposed by Cornell et al. (2002), a linear regression of *EDPs* on *IMs* is established to form PSDMs. Having the PSDMs, the logarithmic correlation between the median estimate of the engineering demand parameter (S_D) and *IM* can be established as given in Eq. (2):

$$\ln(S_D) = \ln(a) + b \ln(IM) \tag{2}$$

The equation above approximates S_D as a function of *IM* values. In addition, $\ln(a)$ and b represent coefficients of the linear regression fitted to given pairs of *EDP-IM*. The model parameter $\ln(a)$ is the vertical intercept, and the parameter b is the slope. The scatter plot of the PSDM portrays the relation between *EDPs* and *IMs* in a log-normal space for each component (e.g., see Figure 12(a)).

The logarithmic standard deviation of S_D conditioned on IM, $\beta_{D|IM}$, is expressed in the following way with respect to the basic statistical formula:

$$\beta_{D|IM} = \sqrt{\sum_{i=1}^{N} [\ln(EDP_i) - \ln(S_D)]^2 (N-2)^{-1}} \tag{3}$$

Where N is the number of ground motions, and EDP_i is the peak demand obtained from NLTHA corresponding to i^{th} ground motion. $\beta_{D|IM}$ is also termed as 'dispersion', that is a dimensionless quantity.

After estimating the demand parameters, S_D and $\beta_{D|IM}$, and adopting a capacity model, S_C and β_C, seismic fragility curves of bridge components conditioned on IM are generated using the following equation:

$$P\{D \geq C|IM\} = 1 - \Phi\left[\frac{\ln(S_C) - \ln(S_D)}{\sqrt{\beta_{D|IM}^2 + \beta_C^2}}\right] \tag{4}$$

where $\Phi[.]$ indicates the standard normal cumulative distribution function. S_C and β_C represent the median and dispersion of the capacity model, which is elaborated in (§5.3).

System-level fragility of bridges can be assessed by integrating component-level fragility curves through the development of joint probabilistic seismic demand models (JPSDMs) (Mangalathu, Jeon, & Jiang, 2019; Nielson, 2005). The JPSDM accounts for correlations between component demands. If $Z = (Z_1, Z_2, \ldots, Z_n)$ denotes the vector of demands on the n components of the bridge in the original space, then $B = \ln(Z)$ represents the corresponding vector of component demands in log-transformed space. The JPSDM is formulated by assembling the mean vector, μ_B, and covariance matrix, σ_B, in the transformed space. The correlation coefficients between component demands are obtained from the NLTHA results. Monte Carlo simulations are employed to generate 10^6 realizations of demand and capacity, enabling probabilistic estimation of demand exceeding capacity for each IM value. This process is repeated for increasing IM values, and regression analysis is used to derive the lognormal parameters (median and dispersion) defining the bridge system fragility curve.

5.2. Earthquake ground motion suite

To obtain the seismic response of bridge components in a probabilistic manner, a set of 40 unscaled standardized ground motions is selected for NLTHAs. The broad-band ground motions were originally proposed by Baker, Lin, and Shahi (2011) for the Transportation Systems Research Program PEER (TSRP). The horizontal response spectra of the set correspond to the median and logarithmic standard deviations predicted for a strike-slip earthquake with a magnitude of 7 on the Richter scale ($M_\omega = 7$) and a seismic source-to-soil distance of 10 km. An average shear wave velocity of 250 m/s has been assumed at a depth of 30 m above the soil layer. The ground motion set accounts for aleatoric uncertainty (record-to-record variability). Various factors may contribute to such uncertainty including the frequency content of ground motions, earthquake magnitudes, and the distance between source and site (Tehrani & Mitchell, 2013). It should be noticed that the orthogonal horizontal pairs of the selected ground motions were mathematically rotated into their fault-normal (FN) and fault-parallel (FP) orientations. Accordingly, they are simultaneously applied to the principal axes of the bridge model in order to perform NLTHAs (e.g., Mangalathu, Jeon, & Jiang, 2019; Noori et al., 2019).

5.3. Limit states

For the development of the fragility function, it is equally important to define limit states of the bridge components (capacity model) as it is to formulate the demand model. Depending on the functional level of the bridge components, the quantity of limit states is determined. Prescriptive approaches based on physics assumptions are used in this process. Four qualitative descriptions of the limit states are apparent: slight, moderate, extensive, and complete. These definitions correspond to those provided by HAZUS qualitative limit states (FEMA, 2003).

Table 2. Bridge *EDPs*, limit state thresholds, and associated structural systems.

Component	Abbr.	*EDPs*	Units	Limit states				Structural system
				Slight S_C	Moderate S_C	Extensive S_C	Complete S_C	
Column curvature	Col	Curvature ductility ($\mu\varphi$)	–	1	5.1	7.5	9	C_1, C_2, C_3, C_4
Longitudinal expansion bearing	LEB	Displacement (δ)	mm	30	100	150	255	C_1, C_2, C_3
Transverse expansion bearing	TEB							C_1, C_2, C_3
Longitudinal fixed bearing	LFB							C_1, C_2, C_3
Transverse fixed bearing	TFB							C_1, C_2, C_3
Elastomeric Bearing	–			25	100	150	255	C_4

Seismic vulnerability assessments mainly focus on two bridge components: columns and bearings. For this purpose, five *EDPs* are defined and used in this research, including curvature ductility demand, μ_φ, for columns, and displacement, δ, for longitudinal and transverse bearings. The limit state quantities for the seismically designed column are adopted from a previous study in terms of curvature ductility (Howard Hwang, Jernigan, & Y-W, 2000; K. Ramanathan, Desroches, & Padgett, 2012). Furthermore, the limit state values related to fixed and expansion bearings are adopted from (K. Ramanathan, Desroches, & Padgett, 2012). Bearings without steel dowels follow the limit state values proposed in Ramanathan's thesis (2012). For simplicity, the same abbreviations are adopted for both dowel-equipped and non-dowel bearings. Table 2 lists these components along with their median values (S_C) and includes the structural system types where these bearings are applied. The dispersion of capacity (β_C) is 0.25 for slight/moderate damage states and 0.47 for extensive/complete limit states.

To calculate μ_φ, the ratio of the maximum curvature (φ_m) to the yield curvature (φ_y) must be determined. Priestley, Seible, and Calvi (1996) proposed a simplified equation to estimate the column yield curvature (φ_y), which is a function of the cross-sectional diameter of the column and the yield strain of the longitudinal reinforcement. In addition, φ_y is calculated using bilinear idealization as recommended by the same researchers. Actually, a decent agreement can be found between the two ($\varphi_y = 0.00485$). It should be mentioned that the square root of sum of squares (SRSS) method is employed to capture the column response.

5.4. Efficient intensity measure

As described, record-to-record (RTR) variability of ground motions brings some levels of inherent randomness into seismic assessment problems (Ellingwood & Wen, 2005; Tehrani & Mitchell, 2013). To this end, the choice of an effective and optimal *IM* can significantly reduce the statistical variations caused by RTR variability. An efficient *IM*, which is just one of the determinants of an optimal *IM* (Giovenale, Cornell, & Esteva, 2004), can minimize the variation in the estimated structural demand. Based on Eq. (3), the most efficient *IM* is determined by the lowest $\beta_{D|IM}$ value (dispersion) among the given *EDP-IM* pairs. This efficiency is explored among three *IMs* including peak ground acceleration (PGA), peak ground velocity (PGV), and spectral acceleration at the intermediate period of the first and second modes of vibration (Sa) (Baker & Cornell, 2006). The geometric mean of the *IM* values for the two horizontal components of each ground motion is regarded as the resultant *IM* (Baker & Cornell, 2006). For Sa, which is a structure-dependent *IM*, the geometric mean of Sa must also be estimated separately for each bridge model. The $\beta_{D|IM}$ values for the components of all the bridge models are calculated with respect to the three explored *IMs*. For instance, the $\beta_{D|IM}$ values associated with the column curvature ductility demand of all the models for the three *IMs* are offered in Figure 10. In this study, PGA is chosen as the efficient *IM* because it showed the highest efficiency in most cases. This choice is also acknowledged by other researchers (e.g., Ghosh, 2021; Padgett & DesRoches, 2008).

The regression coefficients ($\ln(a)$ and (b)) and the coefficient of determination (R^2) are derived for the considered *EDPs* for the 20 models and 3 *IMs*. R^2 exhibits the accuracy of PSDMs, which is a dimensionless quantity. Figure 11(a,b) show the R^2 estimates across the bridge components in the 20 bridge models. Based

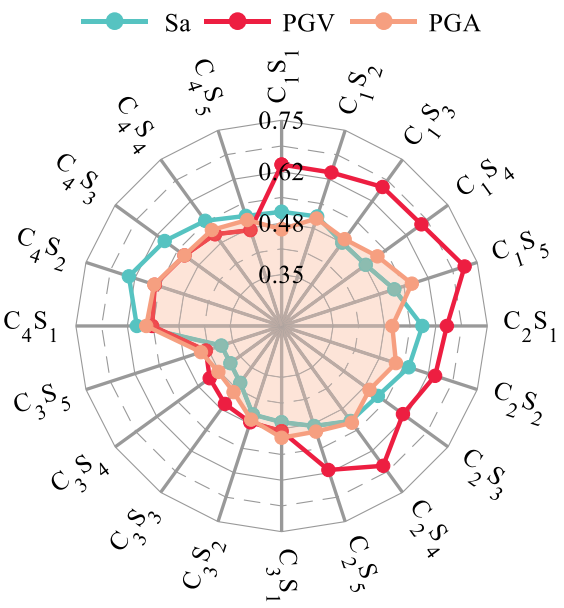

Figure 10. Dispersion ($\beta_{D|IM}$) estimates for the three explored IMs considering column curvature ductility demand as *EDP* across all the bridge models.

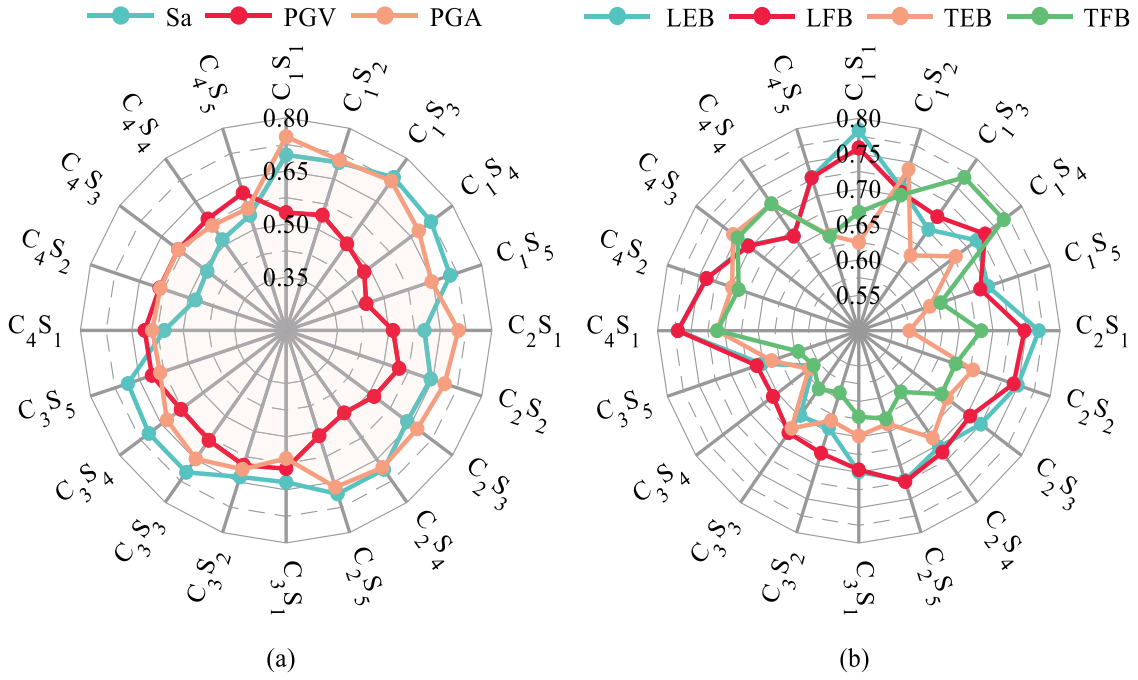

Figure 11. Coefficient of determination (R^2) estimates for all bridge models for (a) Column curvature ductility demand for three different *IMs*, (b) Bearings for PGA as *IM*.

on the figure, the R^2 estimates for the most PSDMs associated with PGA are reasonable, indicating a relatively strong correlation between these *EDPs* and PGA.

A sample of PSDMs related to the column of the C_3S_3 model and the bearings of the C_3S_5 model are displayed in Figure 12(a,b), respectively. The probabilistic seismic demand parameters for the five *EDPs* of two bridge models, C_1S_1 and C_3S_3, are also given in Tables 3–5 with respect to PGA, Sa, and PGV as *IM*, respectively. The tables list the probabilistic seismic demand parameters including $\ln(a)$, b, $\beta_{D|IM}$, and R^2.

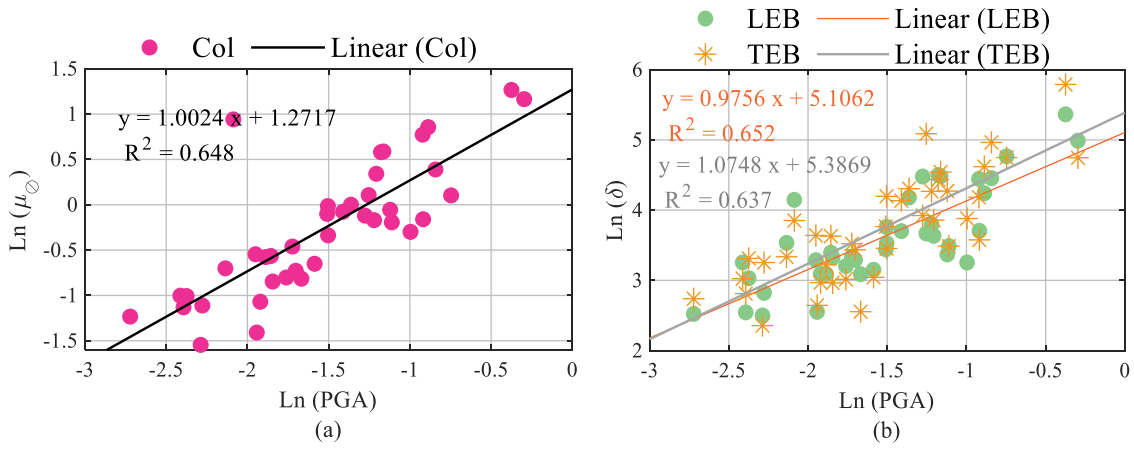

Figure 12. Probabilistic seismic demand models for (a) Column curvature ductility demand corresponding to C_3S_3, (b) Longitudinal and transverse expansion bearings of C_3S_5.

Table 3. Probabilistic seismic demand parameters for bridge components considering PGA as *IM*.

EDPs	Models							
	C_1S_1				C_3S_3			
IM = PGA	Ln(*a*)	*b*	R^2	$\beta_{D\|IM}$	Ln(*a*)	*b*	R^2	$\beta_{D\|IM}$
Col	1.88	1.38	0.74	0.46	1.27	1.00	0.64	0.42
LEB	5.78	1.31	0.78	0.40	5.33	0.99	0.64	0.42
LFB	5.88	1.38	0.75	0.75	5.72	1.43	0.67	0.57
TEB	4.54	1.17	0.62	0.53	5.64	1.63	0.67	0.66
TFB	4.90	1.34	0.66	0.55	5.52	1.57	0.60	0.74

Table 4. Probabilistic seismic demand parameters for bridge components considering Sa as *IM*.

EDPs	Models							
	C_1S_1				C_3S_3			
IM = Sa	Ln(*a*)	*b*	R^2	$\beta_{D\|IM}$	Ln(*a*)	*b*	R^2	$\beta_{D\|IM}$
Col	0.78	1.24	0.69	0.51	0.55	0.94	0.69	0.39
LEB	4.73	1.18	0.72	0.45	4.60	0.92	0.66	0.41
LFB	4.78	1.26	0.71	0.49	4.73	1.40	0.77	0.48
TEB	3.68	1.16	0.69	0.47	4.55	1.64	0.80	0.50
TFB	3.89	1.29	0.70	0.51	4.52	1.63	0.77	0.55

Table 5. Probabilistic seismic demand parameters for bridge components considering PGV as *IM*.

EDPs	Models							
	C_1S_1				C_3S_3			
IM = PGV	Ln(*a*)	*b*	R^2	$\beta_{D\|IM}$	Ln(*a*)	*b*	R^2	$\beta_{D\|IM}$
Col	−3.98	1.10	0.53	0.63	−3.32	0.89	0.58	0.46
LEB	0.12	1.07	0.58	0.56	0.82	0.87	0.56	0.46
LFB	−0.12	1.14	0.57	0.60	−1.04	1.33	0.65	0.59
TEB	−0.18	0.85	0.37	0.68	−1.51	1.36	0.52	0.80
TFB	−0.65	1.02	0.43	0.71	−1.30	1.29	0.46	0.86

6. Results and discussion

This study focuses on the seismic fragility assessment of bridge columns and bearings, considering four various structural systems (i.e., C_1, C_2, C_3, and C_4 as defined in §2) and the five skew angles (i.e., S_1, S_2, S_3, S_4, and S_5). Individual fragility curves of bridge components (columns and bearings) and fragility curves of the system are generated at four damage states: slight, moderate, extensive, and complete. A comparison is made between the seismic fragility curves of the bridge at component- and system-level in the following

subsections (i.e., §6.1.1 and §6.2.1). As the fragility can be investigated by evaluating the relative changes in median PGA values (Abbasi & Moustafa, 2019; K. Ramanathan, Desroches, & Padgett, 2012), a more detailed comparison between the seismic vulnerability of bridge systems based on median PGAs is presented in §6.1.2 and §6.2.2 for the component and system levels, respectively.

6.1. Component-level fragility assessment

6.1.1. Component fragility curves

To study the seismic vulnerability of columns in the various structural systems, their fragility curves are presented in Figure 13(a–d) for the four damage states. More specifically, Figure 13(a) displays the difference between column fragilities at the slight limit state considering different structural systems with S_1. As it can be perceived from the figure, column vulnerability is not significantly influenced by the types of structural systems, particularly for C_3S_1 and C_4S_1 models. The curves of C_3 and C_4 intersect within the range of PGAs, making it difficult to distinguish which structural system is more susceptible to damage. However, appreciable differences can be seen between seismic fragility curves of columns at other limit states (see Figure 13(a–d)). For instance, the probability of the moderate damage to the bridge column in the C_1S_1 model is approximately 77% at PGA = 1 g, whereas it is 18% for the C_3S_1 model (see Figure 13(b)). Referring to Figure 13(a–d), the lowest likelihood of exceeding a given limit state relates to the C_3S_1 model. Besides, the fragility curves of C_1S_1 are above those of the three other models, suggesting that this model is more susceptible to damage than the other models. Similar trends associated with the column fragility have been observed for other skew angles examined in the bridge models.

Figure 14(a,b) illustrates a comparison of fragility curves for two different types of bearings. It can be concluded from the figures that adopting various types of structural systems for bridge affects the seismic

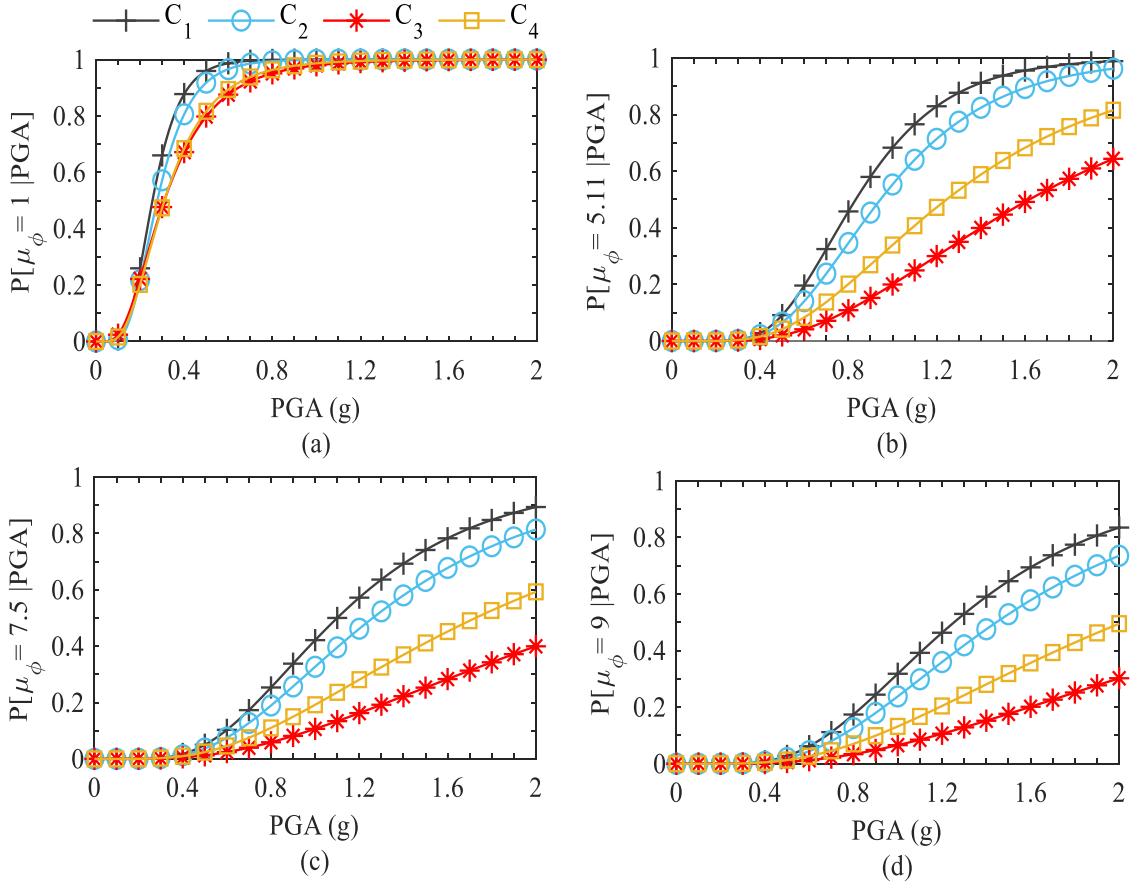

Figure 13. Fragility curves for column curvature ductility demand considering four different structural systems with 0° skew angle at (a) Slight, (b) Moderate, (c) Extensive, and (d) Complete limit states.

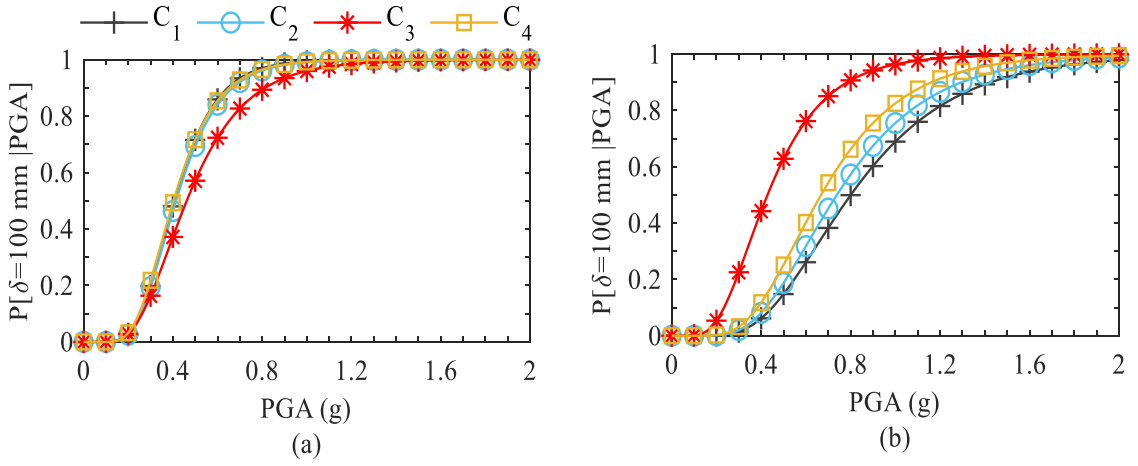

Figure 14. Fragility curves of RC I-girder bridges under the influence of the various assumptions of structural systems for (a) Longitudinal expansion bearing (LEB), (b) Transverse fixed bearing (TFB) - with S_1 at the moderate damage state.

vulnerability of the bearings. The fragility curves of longitudinal expansion bearings are plotted in Figure 14(a) for C_1, C_2, C_3, and C_4 in S_1 at the moderate limit state. This figure shows roughly identical fragilities for longitudinal expansion bearings in C_1, C_2, and C_4. However, this component suggests the lowest fragility for C_3S_1 in comparison to the other structural systems. On the other hand, Figure 14(b) shows that the highest probability of the moderate damage associated with the transverse fixed bearing relates to the C_3S_1 model. Furthermore, the lowest fragility of this component pertains to C_1S_1.

The column fragility curves for skewed RC I-girder bridges are illustrated in Figure 15(a,b) at the moderate limit state. Specifically, the impacts of various skew angles on the vulnerability of bridge columns assuming C_3 is addressed using fragility curves in Figure 15(a). The curves concerning the C_3S_2 and C_3S_3 models demonstrate the highest vulnerability when compared to the rest of the models. Moreover, columns in the C_3S_5 model are less susceptible to the damage than those in the other skewed models. Conversely, the columns of bridges assuming C_1 are less sensitive to variations in the skew angle. The column fragility curves of C_1 are exhibited in Figure 15(b) for scenarios S_1 to S_5. From the comparison of these fragility curves, it can be perceived that the skew angle has a minor impact on the column fragility in C_1 models.

Seismic fragility curves of the five bridge components defined in Table 2 are presented in Figure 16(a–d) at the extensive limit state. Each plot demonstrates fragility curves of a specific structural system with S_4. As indicated in these figures, the column is the least vulnerable component in comparison to the other components. Furthermore, in accordance with Figure 16(b,d), the fragility curves of the fixed and expansion

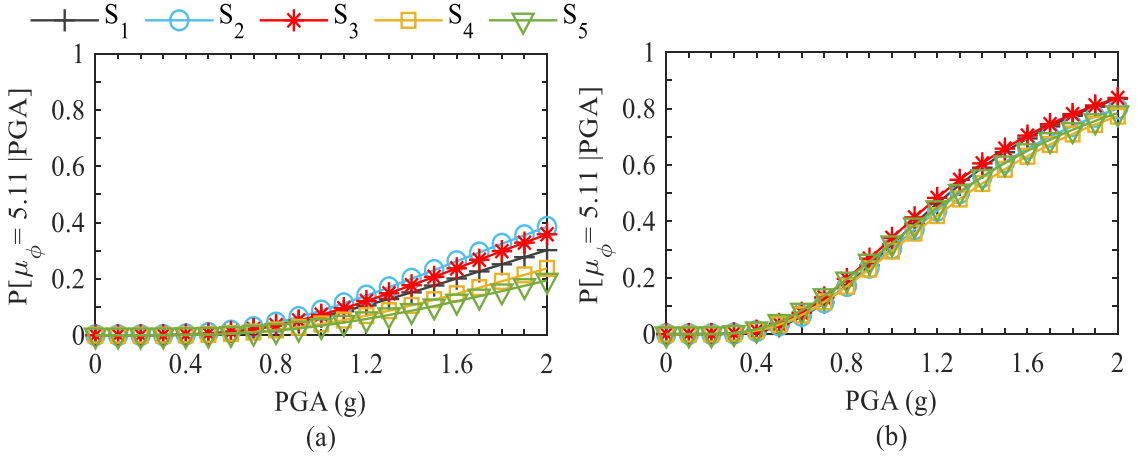

Figure 15. Seismic fragility curves for the column curvature ductility demand across the five different skew angles at the moderate limit state for (a) C_3, (b) C_1 - S_1 to S_5 represent skew angle from 0° to 60° in increments of 15°.

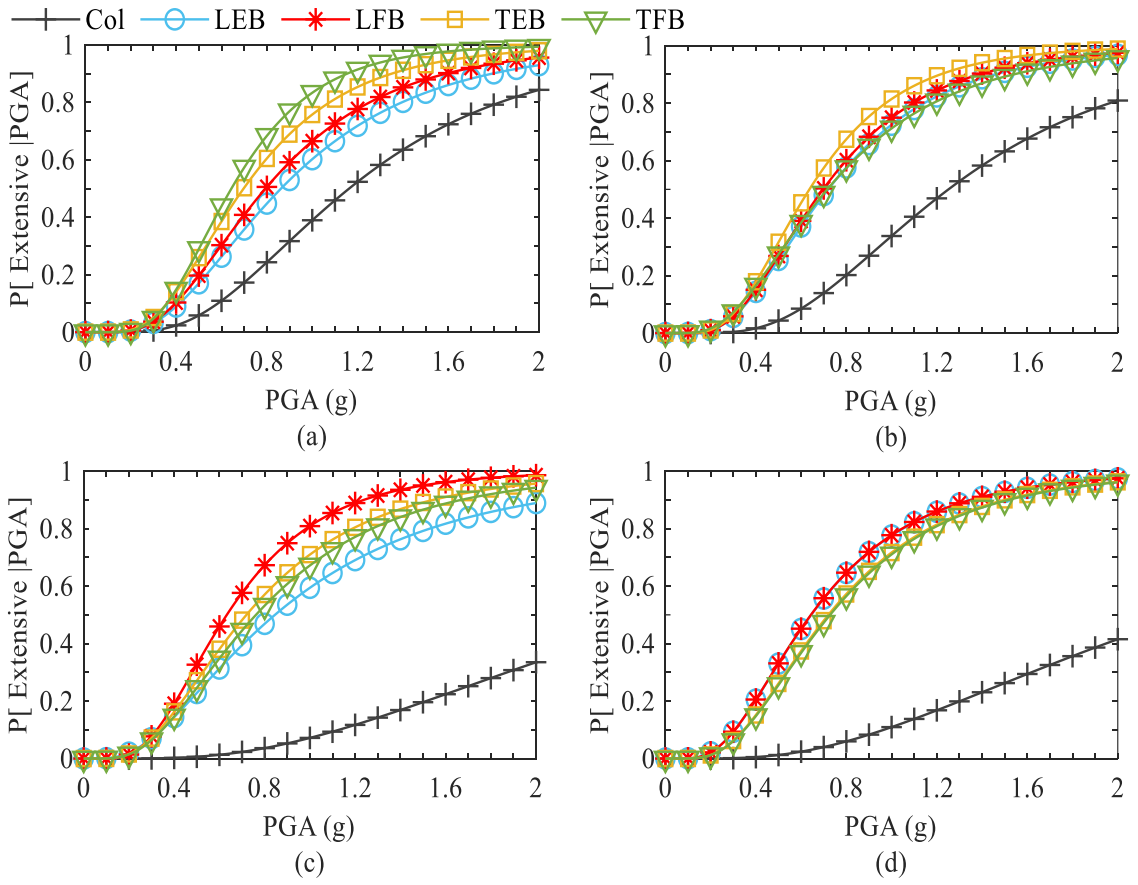

Figure 16. Component seismic fragility curves of bridge for (a) C_1S_4, (b) C_2S_4, (c) C_3S_4, and (d) C_4S_4 - at the extensive limit state.

bearings are quite similar along transverse and longitudinal directions for each model of C_2S_4 and C_4S_4. However, when referring to Figure 16(a,c), the aforementioned components in C_1S_4 and C_3S_4 indicate dissimilar probabilities of damage state exceedance. It is evident that the probability of damage for the column in the four examined limit states in the cases of C_3 and C_4 across five skew angles is the lowest among the five components.

6.1.2. Component fragility medians

This is a relatively straightforward technique to compare differences in the fragility curves. A positive shift in the median PGA value indicates that the bridge components become less fragile, and vice versa. In Figure 17(a–e), the fragility medians at the extensive limit state are illustrated for different bridge components. The median PGAs for columns are depicted in Figure 17(a). The minimum of these values indicates the highest vulnerability, and the maximum of them accounts for the lowest vulnerability. The lowest fragility, concerning column curvature ductility demand, pertains to the C_3S_1 model among the regular bridge models. Apart from C_3S_1, the columns of the C_4S_1, C_2S_1, and C_1S_1 models occupy the second through the fourth places for the lowest vulnerability. For example, the median PGAs for column curvature ductility demand are estimated to be 1.099 g, 1.260 g, 2.389 g, and 1.725 g for the straight bridge model assuming C_1, C_2, C_3, and C_4. In fact, in the cases of C_2, C_3, and C_4, the fragility of the columns decreases by 14.6%, 117.4%, and 56.9% when compared to C_1. The same trend is generally observed for the other three limit states. As shown in Table 6, the impact of different structural systems on column vulnerability is less pronounced at the slight limit state.

According to Figure 17(a), the median PGAs for the columns in straight bridge models of C_1 and C_2 are nearly the same. This can be justified by referring to the fact that including steel dowels in the model of elastomeric bearings increases the stiffness of this type of connection at intermediate bents of the C_2 bridges.

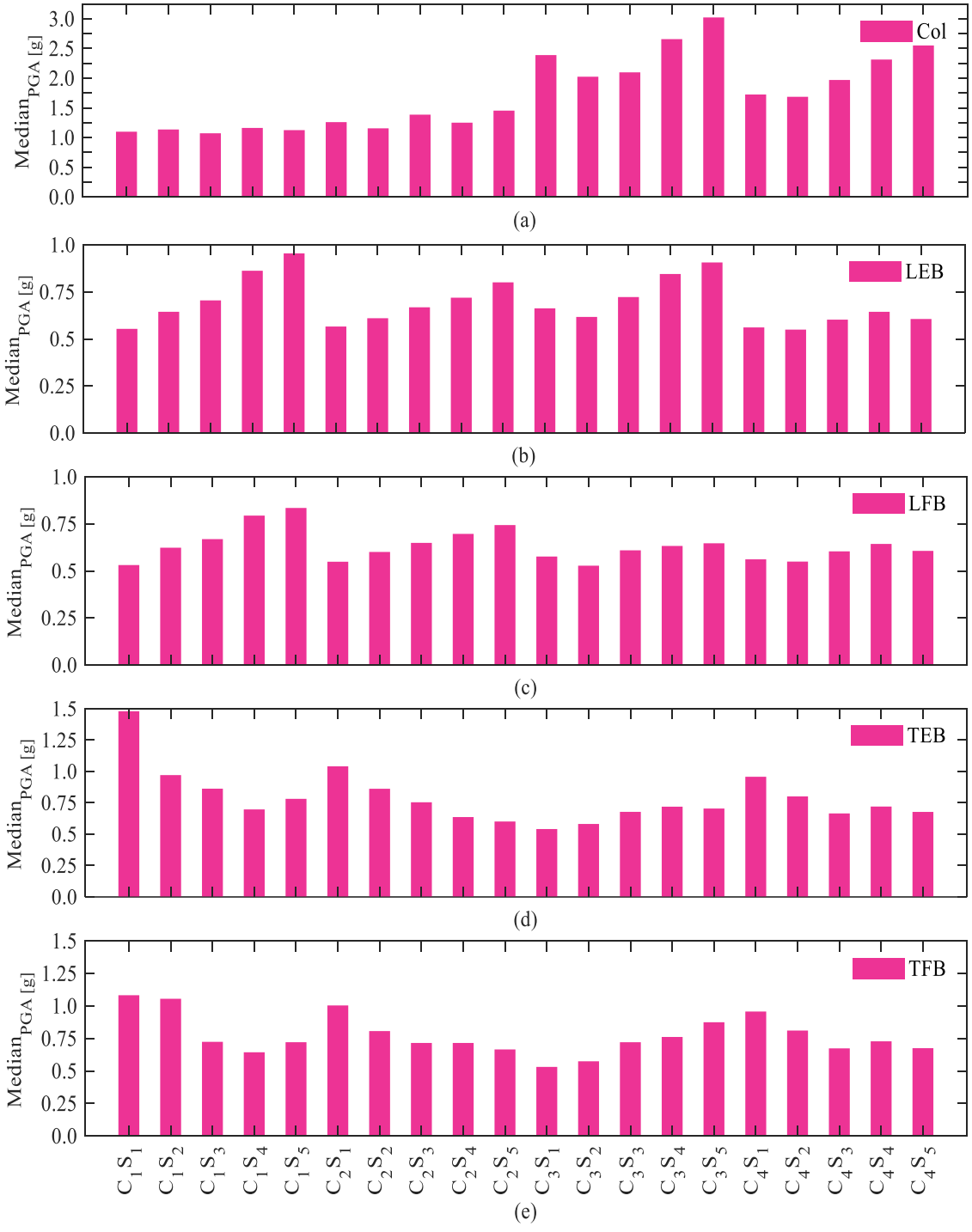

Figure 17. Median PGAs of the obtained fragility functions for the extensive limit state corresponding to (a) Column curvature ductility demand, (b) Longitudinal expansion bearing, (c) Longitudinal fixed bearing, (d) Transverse expansion bearing, and (e) Transverse fixed bearing - S_1 to S_5 represent skew angle from 0° to 60° in increments of 15°.

Therefore, the column fragility of C_2 is fairly close to C_1 where the bent-to-deck connectivity is fully pinned. From another point of view, both models of C_1 and C_2 are free to rotate, but C_1 is totally fixed along translational DOFs, and C_2 is partially restricted at translational DOFs. Nevertheless, the relative change in the column median of PGAs concerning the two structural systems increases when the bridge configuration is modeled with S_5 rather than S_1.

As stated in §3.1, the main difference between model of C_2 and C_4 systems is that elastomeric bearings are modeled together with steel dowels for C_2, while they are modeled alone in the case of C_4. With C_4, the

Table 6. Median PGAs of the obtained fragility functions at slightly damaged state for bridge components.

	Components						Components				
Models	Col	LEB	LFB	TEB	TFB	Models	Col	LEB	LFB	TEB	TFB
C_1S_1	0.26	0.16	0.17	0.38	0.33	C_3S_1	0.31	0.16	0.21	0.23	0.23
C_1S_2	0.26	0.17	0.17	0.30	0.32	C_3S_2	0.28	0.15	0.20	0.24	0.24
C_1S_3	0.25	0.17	0.18	0.27	0.24	C_3S_3	0.28	0.14	0.20	0.25	0.26
C_1S_4	0.25	0.19	0.19	0.23	0.21	C_3S_4	0.31	0.15	0.21	0.22	0.22
C_1S_5	0.25	0.22	0.22	0.19	0.19	C_3S_5	0.32	0.17	0.22	0.16	0.17
C_2S_1	0.28	0.16	0.17	0.30	0.30	C_4S_1	0.31	0.15	0.15	0.23	0.23
C_2S_2	0.26	0.16	0.16	0.27	0.25	C_4S_2	0.29	0.15	0.15	0.20	0.20
C_2S_3	0.27	0.17	0.17	0.23	0.22	C_4S_3	0.31	0.15	0.15	0.17	0.17
C_2S_4	0.27	0.18	0.18	0.21	0.20	C_4S_4	0.33	0.16	0.16	0.16	0.16
C_2S_5	0.28	0.19	0.20	0.19	0.20	C_4S_5	0.33	0.16	0.16	0.14	0.14

Table 7. Median and dispersion values for the bridge system fragility.

Model	S_s*	β_s	S_m	β_m	S_e	β_e	S_c	β_c
C_1S_1	0.117	0.787	0.373	0.724	0.503	0.725	0.742	0.725
C_1S_2	0.118	0.862	0.418	0.796	0.581	0.798	0.885	0.795
C_1S_3	0.122	0.819	0.409	0.753	0.560	0.755	0.834	0.754
C_1S_4	0.122	0.800	0.398	0.733	0.540	0.733	0.796	0.731
C_1S_5	0.112	0.892	0.423	0.821	0.597	0.822	0.914	0.812
C_2S_1	0.117	0.800	0.377	0.736	0.512	0.737	0.763	0.736
C_2S_2	0.113	0.820	0.378	0.764	0.521	0.767	0.791	0.767
C_2S_3	0.111	0.810	0.369	0.748	0.507	0.750	0.767	0.753
C_2S_4	0.113	0.792	0.366	0.732	0.498	0.732	0.746	0.732
C_2S_5	0.112	0.804	0.367	0.738	0.500	0.739	0.750	0.739
C_3S_1	0.113	0.712	0.321	0.608	0.413	0.608	0.574	0.608
C_3S_2	0.108	0.715	0.310	0.618	0.402	0.620	0.564	0.622
C_3S_3	0.112	0.776	0.344	0.723	0.466	0.725	0.692	0.727
C_3S_4	0.111	0.844	0.370	0.778	0.511	0.778	0.778	0.778
C_3S_5	0.106	0.878	0.369	0.807	0.516	0.805	0.797	0.803
C_4S_1	0.109	0.892	0.390	0.820	0.546	0.819	0.847	0.819
C_4S_2	0.102	0.880	0.363	0.813	0.509	0.814	0.792	0.814
C_4S_3	0.101	0.892	0.365	0.826	0.515	0.826	0.807	0.827
C_4S_4	0.096	0.936	0.370	0.867	0.532	0.868	0.857	0.869
C_4S_5	0.095	0.913	0.353	0.848	0.503	0.848	0.800	0.849

*The subscripts *s*, *m*, *e*, *c* denote slight, moderate, extensive, and complete damage states.

columns are less susceptible to damage because the elastomeric bearings are more 'flexible' than the fixed/expansion bearings, and hence, they allow relative movement between the super- and substructure. In other words, the columns of C_4 experience the less curvature demand than C_2. The columns of C_2 sustain higher demand because of the more engaging between the super- and substructure resulting from the fixed/expansion bearings. Furthermore, as elaborated in §2, C_3 is constituted from separated spans, each of which is capable of moving individually. In other words, a smaller portion of deck mass is affected by seismic excitations when compared to the other structural systems. It demonstrates that the seismic demands on columns in C_2S_1 can indeed be larger than those for C_3S_1.

Based on Figure 17(a), the different structural systems affect the seismic response of columns not only in bridge models with skew angle of 0° but also in models with other angles of skewness (i.e., $\theta \neq 0°$). Accordingly, the order of column vulnerability from highest to lowest relates to C_1, C_2, C_4, and C_3. The column median PGAs are 1.125 g, 1.453 g, 2.551 g, and 3.023 g for C_1S_5, C_2S_5, C_4S_5, and C_3S_5, respectively. In other words, C_2S_5, C_4S_5, and C_3S_5 exhibit median PGAs that are 29.1%, 126.7%, and 168.7% greater than C_1S_5. This attests that C_3 renders the least fragility in terms of column curvature ductility, unlike C_1, which is the most fragile. Furthermore, considering skew angles from S_2 to S_5, the similar trends can be found in the moderate and complete limit states as well.

In Figure 17(a), it can be observed that columns in the two structural systems, C_3 and C_4, are sensitive to the angle of skewness. However, it is important to note that this sensitivity diminishes when adopting C_2. The median PGAs corresponding to the curvature ductility demands of columns in C_2, across S_1 to S_5, are 1.260 g, 1.156 g, 1.386 g, 1.254 g, and 1.454 g, respectively. On the other hand, these values for the structural system of C_3 are 2.389 g, 2.025 g, 2.098 g, 2.653 g, and 3.023 g, assuming the same order of skew angles for the bridge. Nonetheless, the figure also exhibits that the lowest fluctuation in median PGAs is given by C_1.

Consequently, the bridge columns of C_1 across five levels of skewness indicate approximately equal fragility median values, unlike C_3 and C_4, which display the most changes in the median PGAs. These trends can also be found at the moderate and complete limit states.

Among all the bridge models investigated in Figure 17(a), the minimum median PGA of 1.072 g is given by the C_1S_3 model, whereas this occurs in other structural systems with S_2, e.g., C_2S_2. Similar results are also observed for the other limit states. Meanwhile, it can be generally resulted, with trivial exceptions such as C_3S_2, that as the angle of skewness is increased, the median PGAs of columns increase, indicating the beneficial role of skewness, especially beyond S_3 for C_3 and C_4 models. In other words, the greater angle of skewness results in the lower vulnerability of columns. To sum up, by increasing skewness, particularly beyond a medium level of angle, the fragility of columns in the cases of C_3 and C_4 diminishes for all the four limit states.

The median PGAs are presented in Figure 17(b–e), corresponding to the extensive damage on the expansion and fixed bearings along longitudinal and transverse directions of the bridge models. It should be noted that the seismic response of bearings is examined at abutments only in the case of the C_1 model, as bent-to-deck connectivity is pinned. Based on Figure 17(b), the median PGAs for the longitudinal expansion bearing of the straight model vary from 0.553 g for C_1 to 0.566 g, 0.662 g, and 0.561 g for C_2, C_3, and C_4, respectively. This indicates that the vulnerability of the longitudinal expansion bearing varies depending on the type of structural system. Additionally, these values for the same component in S_5 are 0.955 g, 0.801 g, 0.906 g, and 0.606 g, revealing the sensitivity of the longitudinal expansion bearing to the skewness. According to Figure 17(c), the longitudinal fixed bearings are also sensitive to the assumptions associated with the structural systems and skewness. Furthermore, a similar conclusion can be drawn at the other limit states. In addition, Figure 17(b,c) illustrates that the longitudinal expansion bearing exhibits lower vulnerability compared to the fixed bearing in the same direction for C_1, C_2, and C_3.

Referring to Figure 17(b,c), despite some exceptions, such as longitudinal bearings of the C_3S_2 model, where fragility peaks out among the other angles, generally, as the skew angle increases, the bearings become less fragile. For example, with reference to Figure 17(c), the fragility medians of 0.548 g, 0.600 g, 0.649 g, 0.698 g, and 0.743 g related to the longitudinal fixed bearing are obtained for C_2S_1, C_2S_2, C_2S_3, C_2S_4, and C_2S_5. It means that by changing the bridge configuration from S_1 to S_5, the probability of attaining the extensive damage to the longitudinal fixed bearings is reduced by 35%. In total, increasing skew angle contributes to the reduction of the fragility of the longitudinal bearings for models with C_1, C_2, C_3, and C_4.

In the cases of C_1, C_2, and C_4, transverse bearing fragility increases as the skew angle increases, in contrast to the other types of bearings. For example, the median PGAs for the transverse expansion bearings of the bridge model with C_2 corresponding to S_1 through S_5 are 1.041 g, 0.862 g, 0.754 g, 0.636 g, and 0.601 g, respectively. However, when C_3 is included in the modeling, the fragility of the transverse bearings decreases as the skewness increases. Referring to Figure 17d, median PGAs of 0.541 g, 0.581 g, 0.678 g, 0.719 g, and 0.704 g are associated with the transverse expansion bearings of the C_3 models from S_1 to S_5, respectively. It means that by switching from C_3S_2 to C_3S_3, a 16.6% reduction in the seismic fragility is achieved. Additionally, these trends concerning the transverse bearings hold true at the moderate and complete limit states for all the structural systems.

It is evident from Figure 17(b–e) that the presence of steel dowel inside the fixed and expansion bearings is a contributing factor in reducing the vulnerability of the bearings. For example, in the case of C_2S_5, the vulnerability of longitudinal expansion bearings is 32.1% lower than that of longitudinal bearings of the C_4S_5 model. Overall, the longitudinal bearings with C_4 are generally more fragile than those of C_2. The trend is consistent across all the damage states.

To compare the seismic vulnerability of the column with that of the bearings, their median PGAs corresponding to the moderate limit state are plotted in Figure 18(a–d) for each structural system versus different skew angles. According to Figure 18(c,d), the bearings are more vulnerable than the columns. It should be noted that the bridge columns of C_3 and C_4 are considerably less vulnerable than the transverse or longitudinal bearings for all the angles of skewness. These results can also be observed at the other limit states. For instance, the fragility medians of the column in C_3 are equal to 1.62 g, 1.39 g, 1.43 g, 1.77 g, and 1.97 g for S_1 to S_5, respectively. The corresponding values for the longitudinal expansion bearings in the same structural system are 0.46 g, 0.43 g, 0.48 g, 0.54 g, and 0.59 g for S_1 to S_5. This means that the seismic vulnerability of the columns for the five skew angles is

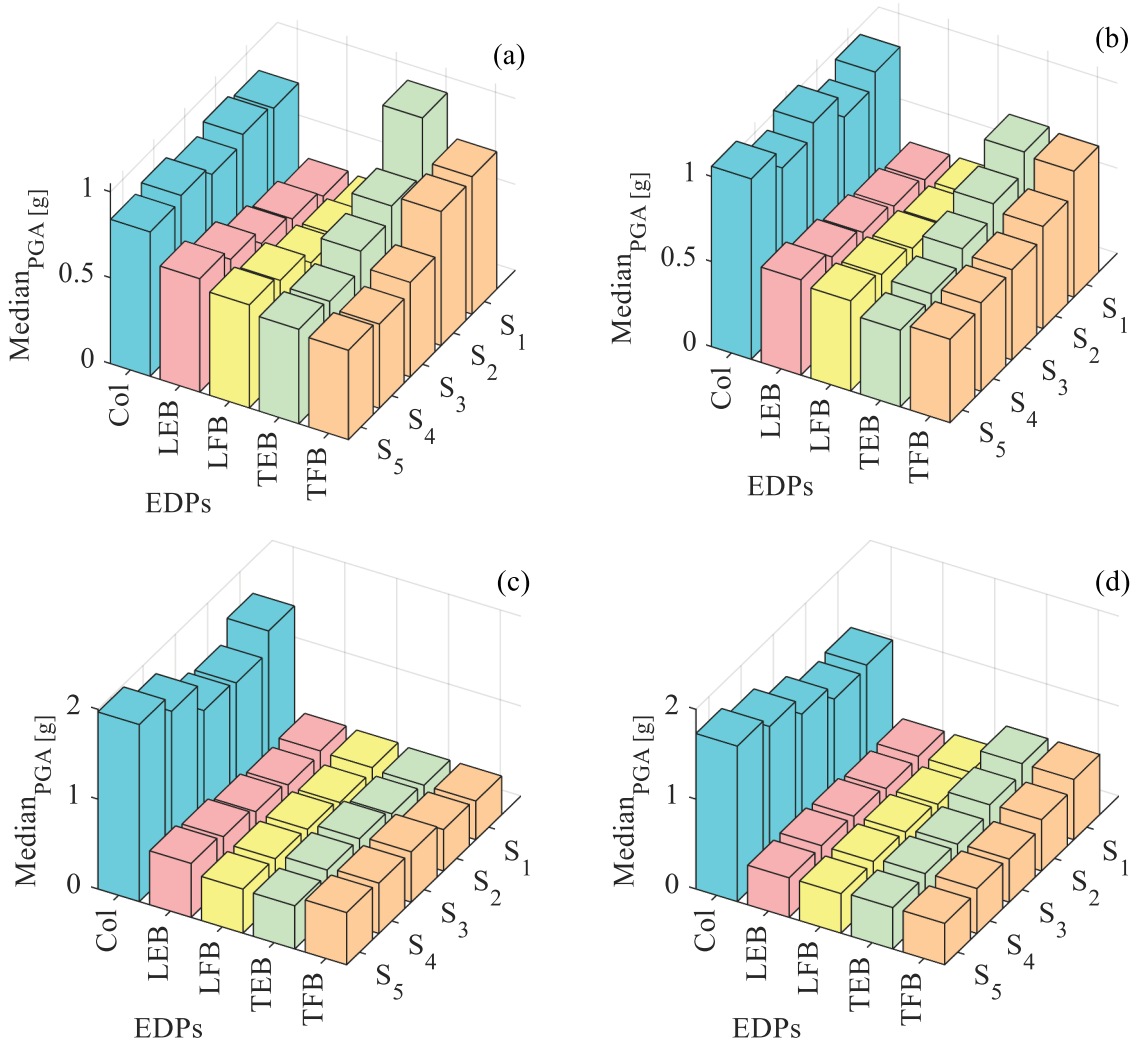

Figure 18. Median PGAs of the obtained fragility functions at the moderate damage state for different bridge components assuming various structural systems: (a) C_1, (b) C_2, (c) C_3, and (d) C_4 versus skew angles - S_1 to S_5 represent skew angle from 0° to 60° in increments of 15°.

by 252.1%, 202.2%, 297.9%, 221.8%, and 228.3% lower compared to that of the longitudinal expansion bearings. Similarly, the vulnerability of the transverse expansion bearings in the C_3 models from S_1 to S_5 is 3.77, 3.02, 2.7, 3.34, and 5.1 times that of the column, respectively. Altogether, the lowest vulnerability at the four limit states and among all the components is given by bridge columns assuming C_3 and C_4.

6.1.3. Fragility median ratios of column curvature ductility

The ratio defined in Eq. (5) is used to comprehend the simultaneous effects of structural systems and skew angles on the seismic fragility of columns across the four limit states. The equation is as follows:

$$R = \frac{median(C_m S_n)}{median(C_1 S_n)} \tag{5}$$

where R is the median PGA of a bridge column obtained for the m^{th} structural system (C_m) divided by that obtained for the model with pinned connection (C_1) at the n^{th} skew angle (S_n).

Figure 19(a–d) illustrates the R ratios for the various models across the four limit states. As evident from comparing the R ratios, columns are strongly influenced by different structural systems at some angles of skewness, e.g., C_2S_4 and C_4S_4 (see Figure 19(a)). However, for certain angles, the figure shows that the

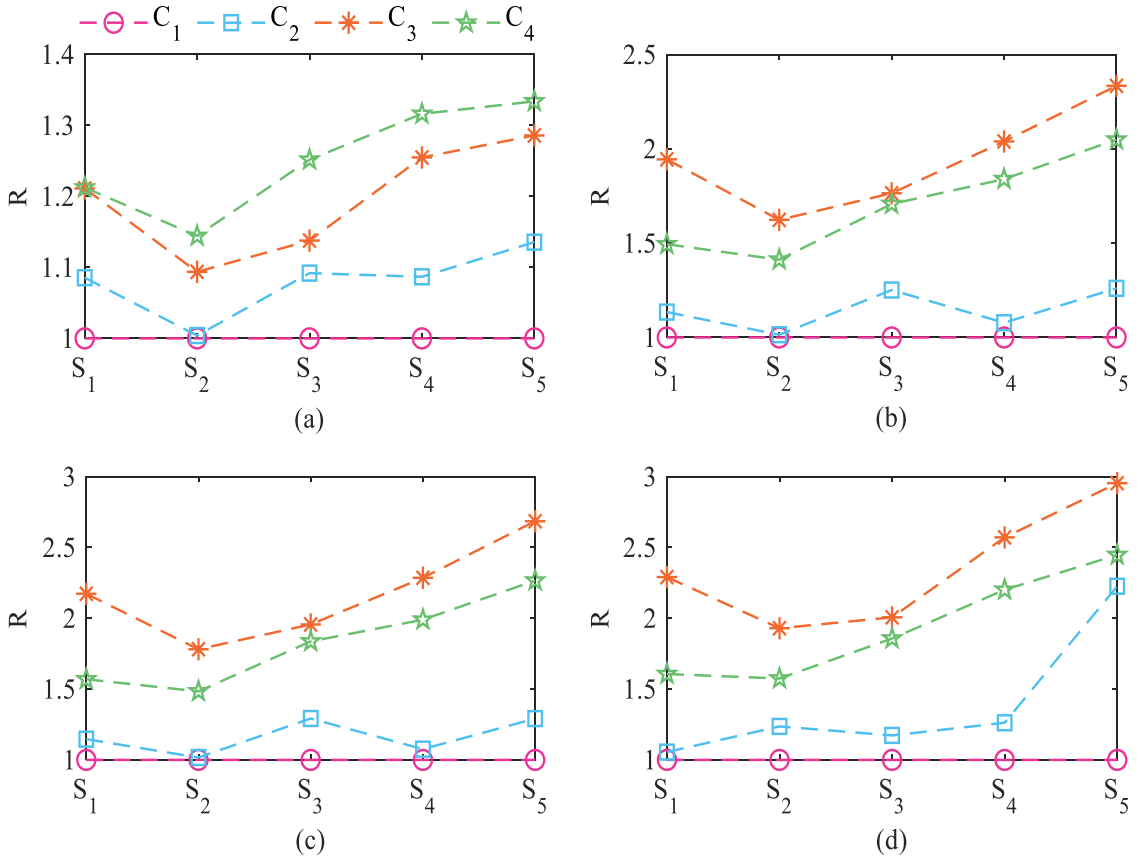

Figure 19. *R* values for different skew angles at (a) Slight, (b) Moderate, (c) Extensive, and (d) Complete limit states.

impacts of different structural systems on column are inconsequential. As a result, the noticeable effects of structural systems on the regular bridge columns may be largely alleviated when considering skewness.

As plotted in Figure 19(a–d), the *R* ratios corresponding to C_3 and C_4 are roughly equal for certain angles. In accordance with Figure 19(c), the *R* ratios of 1.95 and 1.83 pertain to the C_3S_3 and C_4S_3 models. Besides, the *R* ratios for C_1S_2 and C_2S_2 are approximately identical for the three limit states of slight, moderate, and extensive. Although the relative changes in the *R* ratios between C_2 and C_4 are significant at most cases (e.g., 0.76 for S_4 at the moderate limit state), this value is 0.22 in the case of S_5 at the complete damage state. Consequently, a skewed superstructure at certain angles for various limit states may significantly reduce the response sensitivity of columns to the variations of the structural systems.

6.2. System-level fragility assessment

6.2.1. System fragility curves

For the regular bridge ($\theta = 0°$, S_1), the system fragility curves corresponding to the four structural systems examined in this study are presented in Figure 20(a–d) for slight, moderate, extensive, and complete damage states. Comparison of the bridge system fragilities reveals that structural systems C_3 and C_4 exhibit the highest and lowest vulnerability across all damage states. It is observed that the structural systems C_1 and C_2 exhibit similar vulnerability. For instance, at PGA = 1 g, the probability of complete damage reaches 81% for the C_3S_1 model, compared to 58% for C_4S_1 (Figure 20(d)). In contrast, C_1S_1 and C_2S_1 exhibit nearly identical fragility, with probabilities of 65% and 64%. To summarize, for the regular bridges across all limit states, C_4 exhibits the lowest probability of exceedance, whereas C_3S_1 demonstrates the highest vulnerability. In contrast, C_1 and C_2 demonstrate comparable vulnerability.

Figure 21(a,d) presents the bridge system fragility curves across five skew angles (S_1 to S_5 corresponding to skew angles 0° to 60°) at the extensive damage limit state. Figure 21(a) specifically examines the influence of skew angle on the vulnerability of C_3 structural systems. The results

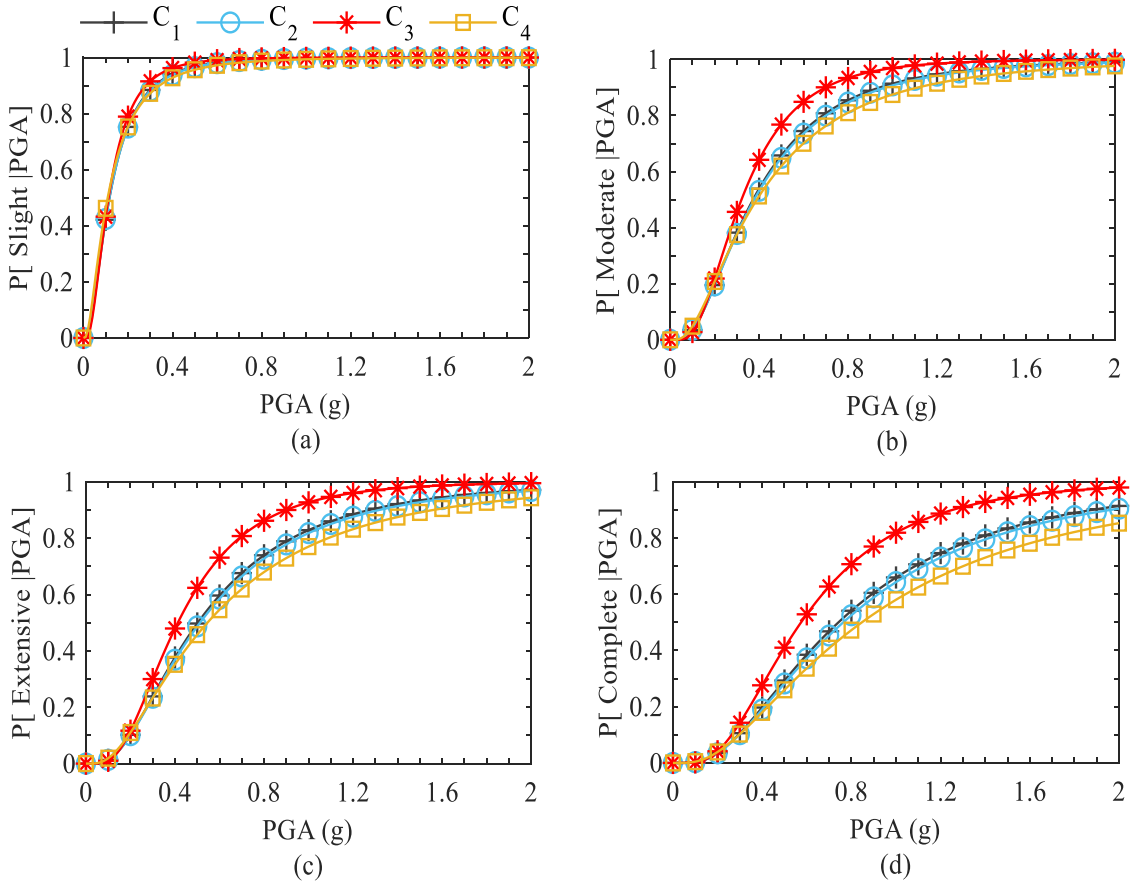

Figure 20. System fragility curves of RC I-girder bridges under the influence of the various assumptions of structural systems with S_1 at (a) Slight, (b) Moderate, (c) Extensive, and (d) Complete limit states.

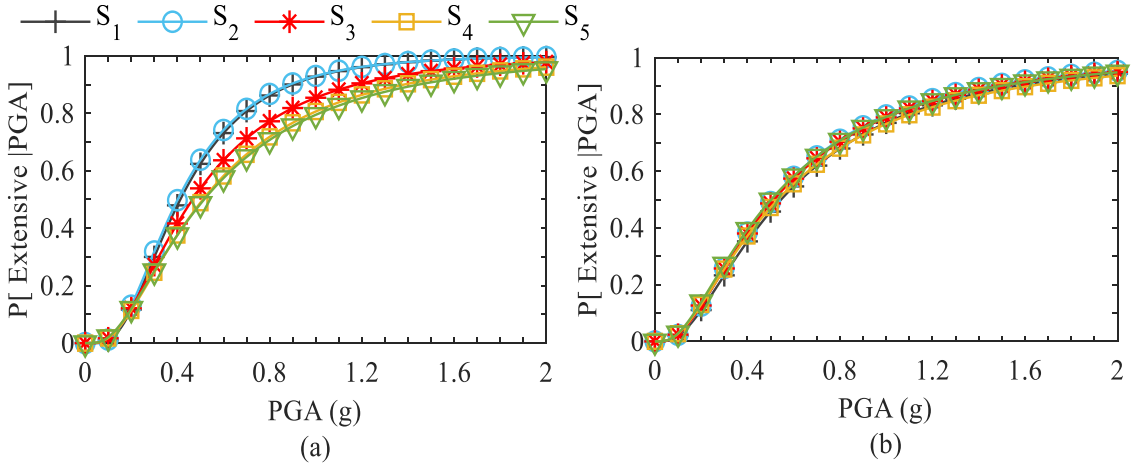

Figure 21. System fragility curves for (a) C_3, (b) C_4 across the five different skew angles at the extensive limit state - S_1 to S_5 represent skew angle from 0° to 60° in increments of 15°.

reveal that the system fragility in C_3 structural systems is sensitive to variations in skew angles. In contrast, Figure 21(b) illustrates the bridge fragility curves for C_4, showing minimal sensitivity to skew angle changes. Findings indicate that the fragility of both C_2 and C_4 is insensitive to skew angle variations, while C_1 and C_3 demonstrate sensitivity across all limit states. The remainder of this section presents and discusses the fragility median values for the bridge system.

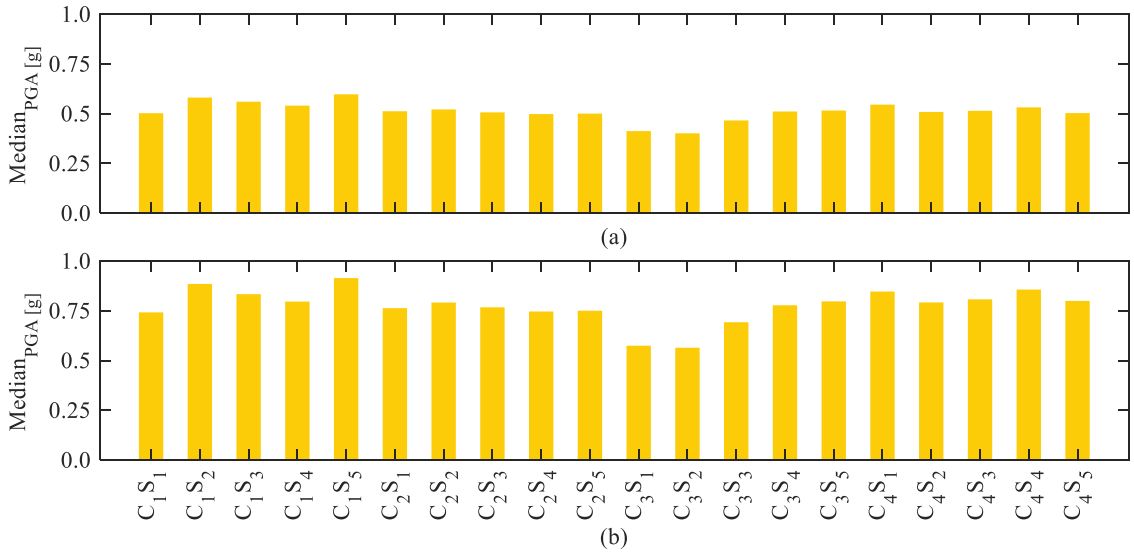

Figure 22. Median PGAs of the obtained system fragility functions across all the bridge models at (a) Extensive, (b) Complete limit states - S_1 to S_5 represent skew angle from 0° to 60° in increments of 15°.

6.2.2. System fragility medians

The parameters of the system fragility functions, i.e., median (S) and dispersion (β), for all bridge models are summarized in **Table 7**. The table indicates similar median PGAs for all bridge models at the slightly damaged state. However, at more severe damage states (extensive and complete), greater variation emerges in the system's fragility medians.

To facilitate direct comparison, Figure 22(a,b) displays the system fragility medians corresponding to the extensive and complete damage states. In Figure 22(a,b), the highest and lowest bridge system fragility pertains to C_3 and C_4 assuming the regular bridge model S_1. The system fragilities of C_1S_1 and C_2S_1 are comparable, falling between the fragility levels of the aforementioned structural systems. For example, the median PGAs for the system fragility at the complete damage state are estimated to be 0.57 g, 0.74 g, 0.76 g, and 0.84 g for the straight bridge model assuming C_3, C_1, C_2, and C_4, respectively. Quantitative comparisons also indicate that C_3 is more vulnerable at S_1 to S_3, compared to alternative systems. In contrast, C_2 shows higher seismic vulnerability at higher skew angles (S_4 and S_5).

As shown in Figure 22(a,b), the influence of skew angle variations on bridge system vulnerability is relatively minor for C_2 and C_4 structural systems at the extensive and complete limit states. Based on the figures, the structural system C_2 is insensitive to variations in skew angles at the extensive damage state, with median fragility values confined to a narrow band between 0.498 g (S_4) and 0.521 g (S_2), varying by less than 5% across all skew angles. However, the system fragility medians of C_1 and C_3 show significantly greater sensitivity to skewness effects at the extensive and complete limit states. At the complete limit state, the median PGAs for the bridge system increase with higher skew angles, exhibiting a 41% variation across the examined range of skew angles (0° to 60°). The study concludes that while bridge skewness can influence the performance of C_1 and C_3 structural systems in the bridge models, its effect on C_2 and C_4 is negligible.

7. Conclusion

This study aims to examine the combined effects of various structural systems and skewness on the seismic behavior of seismically designed multi-span reinforced concrete I-girder bridges. In this respect, the two most common structural systems including multi-span simply supported (C_3) and multi-span continuous girders are considered. The latter structural system in this study is categorized using three different assumptions in terms of boundary conditions including continuous girders with pinned bent-to-deck connectivity (C_1), continuous girders resting on elastomeric bearings along with steel dowels (C_2), and continuous girders resting on elastomeric bearings without steel dowels (C_4).

The results proved that bridge fragility characteristics vary depending on the type of structural system or skew angle under consideration. It is seen that the response sensitivity of the column to the variation of the structural systems may considerably decrease when implementing skewed superstructure. The relative change in fragility medians of the column corresponding to C_3 and C_4 structural systems in the skewed bridges (skew angle of 30°) is about 6 times less than that of the straight bridges (skew angle of 0°). The seismic vulnerability of the column is significantly more pronounced under the effects of skew angles in bridges with the C_3 and C_4 structural systems in comparison to bridges assuming C_1 and C_2. Besides, the skewness plays a beneficial role in reducing the column vulnerability of bridges modeled using C_3 and C_4 structural systems such that, in most cases, the column vulnerability diminishes as the skew angle rises. Given the deployment of different structural systems in the bridges, the order of the column vulnerability from highest to lowest pertains to C_1, C_2, C_4, and C_3. It is also noted that the vulnerability of longitudinal fixed and expansion bearings decreases with increasing skew angles. However, the skewness has an adverse impact on the fragility of transverse fixed and expansion bearings in the bridges with C_1, C_2, and C_4 structural systems. Interestingly, for bridges assuming C_3, as the skew angle increases, the fragility of transverse bearings is actually reduced.

Structural system C_3 exhibits greater system-level vulnerability at lower skew angles (0° to 30°) compared to the other structural systems. In contrast, C_2 is the most vulnerable at higher skew angles. The study concludes that while variation in skew angles can influence the seismic vulnerability of C_1 and C_3 structural systems, its effects on the vulnerability of C_2 and C_4 are negligible.

The findings of this paper highlight that both structural system and skewness angle of bridges can have important implications for post-earthquake recovery, maintenance requirements, and lifecycle performance. Bridges with higher fragility, particularly in key components like columns and bearings, are likely to experience longer downtimes, higher repair costs, and greater disruption to transportation networks. Thus, selecting structural systems with lower fragility (e.g., C_3 in certain skew angles) can contribute to a more resilient infrastructure with reduced recovery times and improved service continuity after seismic events. Future research opportunities include the need to determine the extent to which adopting various self-centering dampers as a retrofit measure can affect the seismic behavior of skewed bridges adopting the different structural systems.

Disclosure statement

No potential conflict of interest was reported by the author(s).

Notes on contributors

Hesam Kiarad received an M.Sc. in Earthquake Engineering from Imam Khomeini International University, specializing in seismic vulnerability assessment of highway bridges. His current research integrates computer technology with civil engineering, focusing on AI applications for structural health monitoring and next-generation sensing systems to enhance infrastructure resilience and sustainable development.

Mohammad Mahdi Memarpour is an Assistant Professor of Civil Engineering at Imam Khomeini International University. His research interests covers seismic fragility assessment of structures—such as tall buildings, highway bridges, and offshore systems—as well as soil-structure interaction.

Soheil Soltanieh received his Ph.D. in Structural Engineering from City, University of London. His research focuses on the development of novel methodologies to enhance the sustainability and robustness of special structures subjected to extreme environmental hazards. His work aims to improve structural performance and resilience through advanced design frameworks addressing uncertainty, system integrity, and long-term reliability.

Panagiotis Elia Mergos is a Senior Lecturer in Structural Engineering at City, University of London. His research focuses on performance-based seismic design optimization and the assessment, retrofit, and resilience of civil structures. His works have been published in top-tier international journals, contributing to advancements in structural engineering theory and practice.

ORCID

P. E. Mergos http://orcid.org/0000-0003-3817-9520

References

Abbasi, M., & Moustafa, M. A. (2017). Effect of shear keys on seismic response of irregular bridge configurations. *Transportation Research Record: Journal of the Transportation Research Board*, *2642*(1), 155–165. https://doi.org/10.3141/2642-17

Abbasi, M., & Moustafa, M. A. (2019). Probabilistic seismic assessment of as-built and retrofitted old and newly designed skewed multi-frame bridges. *Soil Dynamics and Earthquake Engineering*, *119*, 170–186. https://doi.org/10.1016/j.soildyn.2019.01.013

Abbiati, G., Cazzador, E., Alessandri, S., Bursi, O. S., Paolacci, F., & De Santis, S. (2018). Experimental characterization and component-based modeling of deck-to-pier connections for composite bridges. *Journal of Constructional Steel Research*, *150*, 31–50. https://doi.org/10.1016/j.jcsr.2018.08.005

Abdelnaby, A. E., Frankie, T. M., Elnashai, A. S., Spencer, B. F., Kuchma, D. A., Silva, P., & Chang, C.-M. (2014). Numerical and hybrid analysis of a curved bridge and methods of numerical model calibration. *Engineering Structures*, *70*, 234–245. https://doi.org/10.1016/j.engstruct.2014.04.009

Aldea, S., Bazaez, R., Astroza, R., & Hernandez, F. (2021). Seismic fragility assessment of Chilean skewed highway bridges. *Engineering Structures*, *249*, 113300. https://doi.org/10.1016/j.engstruct.2021.113300

Baker, J. W., & Cornell, C. A. (2006). Which spectral acceleration are you using? *Earthquake Spectra*, *22*(2), 293–312. https://doi.org/10.1193/1.2191540

Baker, J. W., Lin, T., & Shahi, S. K. (2011). *New ground motion selection procedures and and Selected Motions for the PEER Transportation Research Program*. Risk Manag.

Bhaskar Panchireddi, S. S., & Ghosh, J. (2023). Influence of ground motion duration on the seismic vulnerability of aging highway bridges. *Structure and Infrastructure Engineering*, *19*(8), 1041–1063. https://doi.org/10.1080/15732479.2021.1998141

Caltrans. (2019). *Caltrans seismic design criteria version 2.0*. California Department of Transportation.

Choi, E. (2002). *Seismic fragility of typical bridges in moderate seismic zones*. Georgia Institute of Technology.

Cornell, C. A., Jalayer, F., Hamburger, R. O., & Foutch, D. A. (2002). Probabilistic basis for 2000 SAC Federal Emergency Management Agency steel moment frame guidelines. *Journal of Structural Engineering*, *128*(4), 526–533. https://doi.org/10.1061/(ASCE)0733-9445(2002)128:4(526)

De Matteis, G., Caprili, S., Carbonari, S., Chisari, C., D'Amato, M., Mattei, F., Zizi, M., Braga, F., Dall'Asta, A., Gara, F., & Salvatore, W. (2022). Critical issues in safety assessment of existing reinforced concrete bridges by means of nonlinear analysis. *Procedia Structural Integrity*, *44*, 681–688. https://doi.org/10.1016/j.prostr.2023.01.089

Ellingwood, B. R., & Wen, Y. K. (2005). Risk-benefit-based design decisions for low-probability/high consequence earthquake events in Mid-America. *Progress in Structural Engineering and Materials*, *7*(2), 56–70. https://doi.org/10.1002/pse.191

Elnashai, A. S., Gencturk, B., Kwon, O. S., Hashash, Y. M. A., Kim, S. J., Jeong, S.-H., & Dukes, J. (2012). The Maule (Chile) earthquake of February 27, 2010: Development of hazard, site specific ground motions and back-analysis of structures. *Soil Dynamics and Earthquake Engineering*, *42*, 229–245. https://doi.org/10.1016/j.soildyn.2012.06.010

Engen, M., Hendriks, M. A. N., Köhler, J., Øverli, J. A., & Åldstedt, E. (2017). A quantification of the modelling uncertainty of non-linear finite element analyses of large concrete structures. *Structural Safety*, *64*, 1–8. https://doi.org/10.1016/j.strusafe.2016.08.003

FEMA. (2003). Hazus-MH MR1: Technical manual. Federal Emergency Management Agency, Washington (DC). https://www.fema.gov/flood-maps/tools-resources/flood-map-products/hazus/user-technical-manuals

Ghosh, J. (2021). Next generation fragility functions for seismically designed highway bridges in moderate seismic zones. *Natural Hazards Review*, *22*(1), 1–19. https://doi.org/10.1061/(ASCE)NH.1527-6996.0000426

Giovenale, P., Cornell, C. A., & Esteva, L. (2004). Comparing the adequacy of alternative ground motion intensity measures for the estimation of structural responses. *Earthquake Engineering and Structural Dynamics*, *33*(8), 951–979. https://doi.org/10.1002/eqe.386

Hou, G., Asce, S. M., Chen, S., & Asce, M. (2017). Bent connection options for curved and skewed SMC bridges in low-to-moderate seismic regions. *Practice Periodical on Structural Design & Construction*, *22*(4), 1–11. https://doi.org/10.1061/(ASCE)SC.1943-5576.0000331

Howard Hwang, B., Jernigan, J. B., & Y-W, L. (2000). Evaluation of seismic damage to Memphis bridges and highway systems. *Journal of Bridge Engineering*, *5*(4), 322–330. https://doi.org/10.1061/(ASCE)1084-0702(2000)5:4(322)

Huo, Y., & Zhang, J. (2013). Effects of pounding and skewness on seismic responses of typical multispan highway bridges using the fragility function method. *Journal of Bridge Engineering*, *18*(6), 499–515. https://doi.org/10.1061/(asce)be.1943-5592.0000414

Ishac, M. G., & Mehanny, S. S. F. (2016). Do mixed pier-to-deck connections alleviate irregularity of seismic response of bridges with unequal height piers? *Bulletin of Earthquake Engineering*, *15*(1), 97–121. https://doi.org/10.1007/s10518-016-9958-8

Jankowski, R. (2015). Pounding between superstructure segments in multi-supported elevated bridge with three-span continuous deck under 3D non-uniform earthquake excitation. *Journal of Earthquake and Tsunami*, *9*(4), 1–18. https://doi.org/10.1142/S1793431115500128

Kabir, M. R., Billah, A. H. M. M., & Alam, M. S. (2019). Seismic fragility assessment of a multi-span RC bridge in Bangladesh considering near-fault, far-field and long duration ground motions. *Structures*, *19*, 333–348. https://doi.org/10.1016/j.istruc.2019.01.021

Kaviani, P., Zareian, F., & Taciroglu, E. (2012). Seismic behavior of reinforced concrete bridges with skew-angled seat-type abutments. *Engineering Structures*, *45*, 137–150. https://doi.org/10.1016/j.engstruct.2012.06.013

Maleki, S. (2005). Seismic modeling of skewed bridges with elastomeric bearings and side retainers. *Journal of Bridge Engineering*, *10*(4), 442–449. https://doi.org/10.1061/(asce)1084-0702,(2005)10:4(442)

Mander, J. B., Priestley , M. J. N., & Park, R. (1988). Theoretical stress-strain model for confined concrete. *Journal of Structural Engineering*, *114*(8), 1804–1826. https://doi.org/10.1061/(ASCE)0733-9445(1988)114:8(1804)

Mangalathu, S., Jeon, J.-S., & Jiang, J. (2019). Skew adjustment factors for fragilities of California box-girder bridges subjected to near-fault and far-field ground motions. *Journal of Bridge Engineering*, *24*(1), 04018109. https://doi.org/10.1061/(asce)be.1943-5592.0001338

McKenna, F. (2011). Opensees: A framework for earthquake engineering simulation. *Computing in Science & Engineering*, *13*(4), 58–66. https://doi.org/10.1109/MCSE.2011.66

Miner, L. R. (2014). Effect of abutment skew and horizontally curved alignment on bridge reaction forces. [M.Sc. thesis]. California State University, Sacramento. http://hdl.handle.net/10211.3/122036

Mirzai, N. M., Eslamnia, H., Bakhshinezhad, S., & Jeong, S.-H. (2023). Seismic fragility assessment of a multi-span continuous I-girder bridge controlled by a self-centering damper. *Structures*, *50*, 1838–1856. https://doi.org/10.1016/j.istruc.2023.02.091

Muthukumar, S., & DesRoches, R. (2006). A Hertz contact model with non-linear damping for pounding simulation. *Earthquake Engineering and Structural Dynamics*, *35*(7), 811–828. https://doi.org/10.1002/eqe.557

Nielson, B. G. (2005). *Analytical fragility curves for highway bridges in moderate seismic zones* [Ph.D. thesis]. Georgia Institute ofTechnology.

Noori, H. R., Memarpour, M. M., Yakhchalian, M., & Soltanieh, S. (2019). Effects of ground motion directionality on seismic behavior of skewed bridges considering SSI. *Soil Dynamics and Earthquake Engineering*, *127*, 105820. https://doi.org/10.1016/j.soildyn.2019.105820

Omranian, E., Abdelnaby, A. E., & Abdollahzadeh, G. (2018). Seismic vulnerability assessment of RC skew bridges subjected to mainshock-aftershock sequences. *Soil Dynamics and Earthquake Engineering*, *114*, 186–197. https://doi.org/10.1016/j.soildyn.2018.07.007

Padgett, J. E., & DesRoches, R. (2008). Methodology for the development of analytical fragility curves for retrofitted bridges. *Earthquake Engng. Struct. Dyn.,* 37, 1157–1174. https://doi.org/10.1002/eqe.801

Priestley, M. J. N., Seible , F., & Calvi, G.M. (1996). *Seismic design and retrofit of bridges*. John Wiley & Sons, Ince.

Ramanathan, K., Desroches, R., & Padgett, J. E. (2012). A comparison of pre- and post-seismic design considerations in moderate seismic zones through the fragility assessment of multispan bridge classes. *Engineering Structures*, *45*, 559–573. https://doi.org/10.1016/j.engstruct.2012.07.004

Ramanathan, K. N. (2012). *Next generation seismic fragility curves for California bridges incorporating the evolution in seismic design philosophy*. Georgia Institute of Technology.

Rezaei, H., Mohammadi Dehcheshmeh, E., & Tsompanakis, Y. (2025). Impact of analysis method on the fragility curves of regular and irregular box-girder highway bridges. *Structure and Infrastructure Engineering*, *0*, 1–21. https://doi.org/10.1080/15732479.2025.2491836

Saiidi, M. S., Vosooghi, A., & Nelson, R. B. (2013). Shake-table studies of a four-span reinforced concrete bridge. *Journal of Structural Engineering*, *139* (8), 1352–1361. https://doi.org/10.1061/(asce)st.1943-541x.0000790

Shamsabadi, A., & Rollins, K. M. (2014). Three-dimensional nonlinear continuum seismic soil-structure interaction analysis of skewed bridge abutments. *Numerical Methods in Geotechnical Engineering - Proceedings of the 8th European Conference on Numerical Methods in Geotechnical Engineering (NUMGE 8)*, *2*, 933–938. https://doi.org/10.1201/b17017-166

Shekhar, S., Ghosh, J., & Ghosh, S. (2022). Influence of bearing types and design code advances on seismic vulnerability of simply supported highway bridges. *Journal of Earthquake Engineering*, *26*(10), 4977–5003. https://doi.org/10.1080/13632469.2020.1852138

Soleimani, F., Vidakovic, B., DesRoches, R., & Padgett, J. (2017). Identification of the significant uncertain parameters in the seismic response of irregular bridges. *Engineering Structures*, *141*, 356–372. https://doi.org/10.1016/j.engstruct.2017.03.017

Soltanieh, S., Memarpour, M. M., & Kilanehei, F. (2019). Performance assessment of bridge-soil-foundation system with irregular configuration considering ground motion directionality effects. *Soil Dynamics and Earthquake Engineering*, *118*, 19–34. https://doi.org/10.1016/j.soildyn.2018.11.006

Somala, S. N., Karthik Reddy, K. S. K., & Mangalathu, S. (2021). The effect of rupture directivity, distance and skew angle on the collapse fragilities of bridges. *Bulletin of Earthquake Engineering*, *19*(14), 5843–5869. https://doi.org/10.1007/s10518-021-01208-8

Sullivan, I., & Nielson, B. G. (2010). Sensitivity analysis of seismic fragility curves for skewed multi-span simply supported steel girder bridges. *Proceedings of the 19th Analytical Computational Special Conference*, 226–237. https://doi.org/10.1061/41131(370)19

Sun, D., Dai, J., Huang, Y., & Huang, S. (2023). Comparative experimental study on shaking table test of small radius curved bridge considering different connection types between pier and beam. *Strcuctures*, *58*, 105612. https://doi.org/10.1016/j.istruc.2023.105612

Tehrani, P., & Mitchell, D. (2013). Incremental dynamic analysis (IDA) applied to seismic risk assessment of bridges; 561–596. Elsevier. https://doi.org/10.1533/9780857098986.4.561

Terzic, V., & Stojadinovic, B. (2015). Calibration and validation of analytical models for predicting the seismic and axial-load response of circular bridge columns. *Journal of Bridge Engineering*, *20*(9), 04014098. https://doi.org/10.1061/(asce)be.1943-5592.0000702

Wen, Y. K., Ellingwood, B. R., Veneziano, D., & Bracci, J. (2003). *Uncertainty modeling in earthquake engineering*. MAE Cent Proj.

Yang, C. S. W., Werner, S. D., & DesRoches, R. (2015). Seismic fragility analysis of skewed bridges in the Central Southeastern United States. *Engineering Structures*, *83*, 116–128. https://doi.org/10.1016/j.engstruct.2014.10.025

Zakeri, B., & Ghodrati Amiri, G. (2014). Probabilistic performance assessment of retrofitted skewed multi span continuous concrete i-girder bridges. *Journal of Earthquake Engineering*, *18*(6), 945–963. https://doi.org/10.1080/13632469.2014.916241

Zakeri, B., Padgett, J. E., & Amiri, G. G. (2014). Fragility analysis of skewed single-frame concrete box-girder bridges. *Journal of Performance of Constructed Facilities*, *28*(3), 571–582. https://doi.org/10.1061/(asce)cf.1943-5509.0000435

Zakeri, B., & Zareian, F. (2018). Design of bridges with skewed abutments for a target tolerable seismic loss. *Engineering Structures*, *164*, 325–334. https://doi.org/10.1016/j.engstruct.2018.02.020